universität wien

MASTERARBEIT | MASTER'S THESIS

Titel | Title

Exploring adaptive resistance mechanisms towards BRAF inhibitors in pediatric high-grade gliomas
Integrative analysis of genetic alterations and gene expression profiles with Next-Generation Sequencing

verfasst von | submitted by
Patrizia Gurschka BSc

angestrebter akademischer Grad | in partial fulfilment of the requirements for the degree of
Master of Science (MSc)

Wien | Vienna, 2025

Studienkennzahl lt. Studienblatt | Degree programme code as it appears on the student record sheet:	UA 066 910
Studienrichtung lt. Studienblatt | Degree programme as it appears on the student record sheet:	Masterstudium Computational Science
Betreut von | Supervisor:	Univ.-Prof. Dr. Christopher Gerner

This master thesis was supervised externally by:

Lisa Gabler, PhD, MSc, BSc, BSc

at the

Neurosurgical Research Lab

Department of Neurosurgery

Medical University Vienna

in cooperation with the

Center of Cancer Research

Medical University Vienna

Acknowledgements

I want to thank my external supervisor, Lisa Gabler, sincerely for her support, valuable insights, and constructive feedback throughout the development of this thesis. Her guidance, patience, and encouragement have been incredibly helpful, and I truly appreciate the time and effort she dedicated to mentoring me.

A big thank you also goes to everyone else who supported me along the way - whether through academic discussions, helpful feedback, or simply by keeping me motivated. In particular, I want to express my gratitude to the Berger-Heffeter research group at the Center of Cancer Research and the Neurosurgical Research Lab at the Department of Neurosurgery of the Medical University Vienna for their invaluable input, collaboration, and the inspiring research environment.

I am especially grateful to my friends and family for their encouragement, patience, and for always having my back during stressful times.

Abstract

Pediatric high-grade gliomas are amongst the most aggressive tumors of the central nervous system in children. High-grade gliomas make up around 40% of all deaths associated with brain tumors in children. The five-year survival rate for children suffering from high-grade gliomas is 28.4% despite the multimodal treatment. A subgroup of pediatric high-grade gliomas is characterized by *BRAF V600E* gain-of-function mutations leading to constitutive activation of the MAPK signaling pathway and increased cancer cell proliferation, dedifferentiation, and survival. Therefore, targeted therapy with BRAF inhibitors was approved for clinical use. Although BRAF inhibitors such as dabrafenib initially show promising results in patients, their efficacy diminishes over treatment duration due to acquired resistance mechanisms. Here, we thought to investigate the underlying resistance mechanisms on a molecular level and possible alternative treatment options using a multi-omic approach.

Three cell models of a pediatric patient with high-grade glioma, originating from the primary and recurrent lesion, as well as one *in vitro*-generated dabrafenib-resistant subline of the recurrent model, were used characterized using two-color microarrays, RNA sequencing, and whole exome sequencing.

The presence of the *BRAF V600E* mutation was verified in all three cell models. Analysis of the most frequently described resistance mechanism against BRAF inhibitors in *BRAF V600E*-mutated high-grade gliomas, reactivation of the MAPK pathway, revealed that important genes involved in the MAPK pathway are downregulated, indicating that this

signaling pathway is less active in our resistant cell model compared to the recurrent model. Downregulated gene set variation and enrichment analyses (GSVA and GSEA) results of pathways relating to the MAPK pathway confirmed the gene downregulation. Investigation of missense mutations in our whole exome sequencing data detected mutations directly affecting the MAPK pathway, influencing cell differentiation, proliferation, and survival or impacting BRAF inhibitor efficacy and tumor cell interactions, leading to independence of the MAPK pathway due to acquired mutations. Examination of expression array and RNA sequencing data showed lower expression of genes involved in negative regulation of the PI3K/AKT/mTOR pathway. Therefore, alternative activation of the PI3K/AKT/mTOR pathway seems to be a potential resistance mechanism in our dabrafenib-resistant cell model. Furthermore, we detected significant upregulation of *ABCB1* in the dabrafenib-resistant cell model, indicating overexpression of drug efflux pumps leading to challenges in drug delivery.

A large-scale drug screen revealed hypersensitivity of our resistant subline to platinum-based compounds (cisplatin, oxaliplatin, carboplatin). GSEA indicated significant downregulation of DNA repair and DNA damage response pathways, and upregulation of TP53 signaling, suggesting impaired DNA damage response.

In summary, our findings propose that BRAF inhibitor resistance in our resistant model is driven by alternative PI3K/AKT/mTOR pathway activation, MAPK pathway independence via acquired mutations, and increased drug efflux. Furthermore, the observed impaired DNA repair mechanisms may explain an increased vulnerability to platinum-based compounds, which represents a promising alternative therapeutic strategy in BRAF inhibitor-resistant high-grade gliomas.

Kurzfassung

Pädiatrische hochgradige Gliome gehören zu den aggressivsten Tumoren des zentralen Nervensystems bei Kindern. Sie sind für etwa 40% aller Todesfälle im Zusammenhang mit Hirntumoren bei Kindern verantwortlich. Trotz multimodaler Therapie beträgt die Fünf-Jahres-Überlebensrate von Kindern mit hochgradigen Gliomen nur 28.4%. Eine Untergruppe dieser Tumoren ist durch die aktivierende *BRAF V600E*-Mutation gekennzeichnet, welche zu einer konstitutiven Aktivierung des MAPK-Signalweges führen und eine erhöhte Krebszellenproliferation, Dedifferenzierung und Überlebensfähigkeit begünstigen. Daher wurde eine gezielte Therapie mit BRAF Inhibitoren für den klinischen Einsatz zugelassen. Obwohl BRAF Inhibitoren wie Dabrafenib anfangs vielversprechende Ergebnisse zeigen, nimmt ihre Wirksamkeit im Laufe der Behandlung aufgrund erworbener Resistenzmechanismen ab. In dieser Studie untersuchten wir die zugrunde liegenden Resistenzmechanismen auf molekularer Ebene, sowie mögliche alternative Behandlungsoptionen mittels eines multi-omischen Ansatzes.

Drei Zellmodelle eines pädiatrischen Patienten mit hochgradigem Glioma, die aus der Primär- und Rezidivläsion stammen, sowie eine *in vitro* generierte Dabrafenib-resistente Sublinie des Rezidivmodells, wurden mittels Zwei-Farben-Microarrays, RNA Sequenzierung und Exom-Sequenzierung charakterisiert.

Das Vorhandensein der *BRAF V600E*-Mutation wurde mit dem Integrative Genomics Viewer in allen drei Zellmodellen bestätigt. Die Analyse des häufigsten Resistenzmechanismus gegen BRAF Inhibitoren in *BRAF V600E*-mutierten hochgradigen Gliomen - die

Kurzfassung

Reaktivierung des MAPK-Signalweges - ergab, dass wichtige Gene dieses Signalweges herunterreguliert sind. Dies deutet darauf hin, dass der MAPK-Signalweg in unserem resistenten Zellmodell im Vergleich zum Rezidivmodell weniger aktiv ist. Die Ergebnisse der Gen-Set-Variation- und Gen-Set-Enrichment-Analyse von den Signalwegen, die mit dem MAPK-Signalweg in Verbindung stehen, bestätigen diese Gen-Herunterregulation. Die Untersuchung von Missense-Mutationen in unseren Exom-Sequenzierungsdaten identifizierte Mutationen, die den MAPK-Sigalweg direkt beeinflussen, Zell-Differenzierung, Proliferation sowie Überlebensfähigkeit verändern oder die Wirksamkeit von BRAF Inhibitoren und Tumor-Zell-Interaktionen beeinflussen, das zu einer Unabhängigkeit vom MAPK-Signalweg durch erworbene Mutationen führt. Die Analyse von Expressionsdaten aus Microarrays und RNA Sequenzierungen zeigte eine geringere Expression von Genen, die für die negative Regulation des PI3K/AKT/mTOR-Signalweges wichtig sind. Dies deutet darauf hin, dass die alternative Aktivierung des PI3K/AKT/mTOR-Signalweges ein potenzieller Resistenzmechanismus in unserem Dabrafenib-resistenten Zellmodell darstellt. Zusätzlich stellten wir eine signifikante Hochregultation von *ABCB1* in unserem Dabrafenib-resistenten Zellmodell fest. Dies weist auf eine Überexpression von Arzneimittel-Efflux-Pumpen hin, die den Arzneimitteltransport im Tumor einschränken könnten.

Ein groß angelegtes Wirkstoff-Screening zeigte eine Überempfindlichkeit unserer resistenten Sublinie gegenüber platinbasierten Verbindungen (Cisplatin, Oxaliplatin, Carboplatin). Die GSEA ergab eine signifikante Herunterregulation von Signalwegen, die mit der DNA-Reparatur und der Reaktion auf DNA-Schäden assoziiert sind, sowie eine Hochregulation der TP53-Signalgebung, das auf eine beeinträchtigte Reaktion auf DNA-Schäden hindeutet.

Zusammenfassend, legen unsere Ergebnisse nahe, dass die Resistenz gegen BRAF Inhibitoren in unserem resistenten Modell durch die alternative Aktivierung des PI3K/AKT/mTOR-Signalweges, eine Unabhängigkeit von MAPK-Signalweg aufgrund erworbener Mutationen

und eine verstärkte Wirkstoff-Efflux-Aktivität bedingt ist. Darüber hinaus könnten die beobachteten defekten DNA-Reparaturmechanismen eine erhöhte Empfindlichkeit gegenüber platinbasierten Wirkstoffen erklären, welche eine vielversprechende alternative Therapiestrategie für BRAF Inhibitor-resistente hochgradige Gliome darstellen könnte.

Inhaltsverzeichnis

1. Introduction

1.1. Biological background

Pediatric brain cancers

Brain cancers are the most common solid tumors and the leading cause of cancer-related death in children (Price et al., 2024).

The prognosis of pediatric brain cancer patients depends on the tumor location, time of diagnosis, and the tumor type and is therefore highly variable. Although the causes for cancers in children are often unclear, germline gene aberrations involving mutations or deletions may predispose many pediatric patients for certain cancers. Other risk factors involve long-term or high amount of radiation exposure, for example through X-rays or previous radiation therapy (American Childhood Cancer Organization, 2018).

Children with brain cancer may present in the clinics with symptoms like headaches, recurrent nausea and vomiting, and sensory function deficits, including hearing, speech, and vision. Pediatric brain cancer patients often experience impaired mobility, difficulties with balance and coordination, and may also suffer from seizures, reflecting the impact of tumor location and associated neural dysfunctions. Usually changes in behavior, personality, and activity level as well as an unusual amount of sleep are observed (PDQ Pediatric Treatment Editorial Board, 2019). When such symptoms are witnessed, a complete medical history, a physical, and a neurological exam are performed to check the patient's physical performance and brain function. Computed tomography (CT) and

magnet resonance imaging (MRI) scans are the most common and sensitive radiographic methods testing for brain diseases (PDQ Pediatric Treatment Editorial Board, 2019). Brain cancers can be categorized into more than 150 specific entities, which are differentiated based on molecular features and histological characteristics. Also, radiographically tumors show distinct heterogeneity in their structure and size, and location in the brain (Louis et al., 2021).

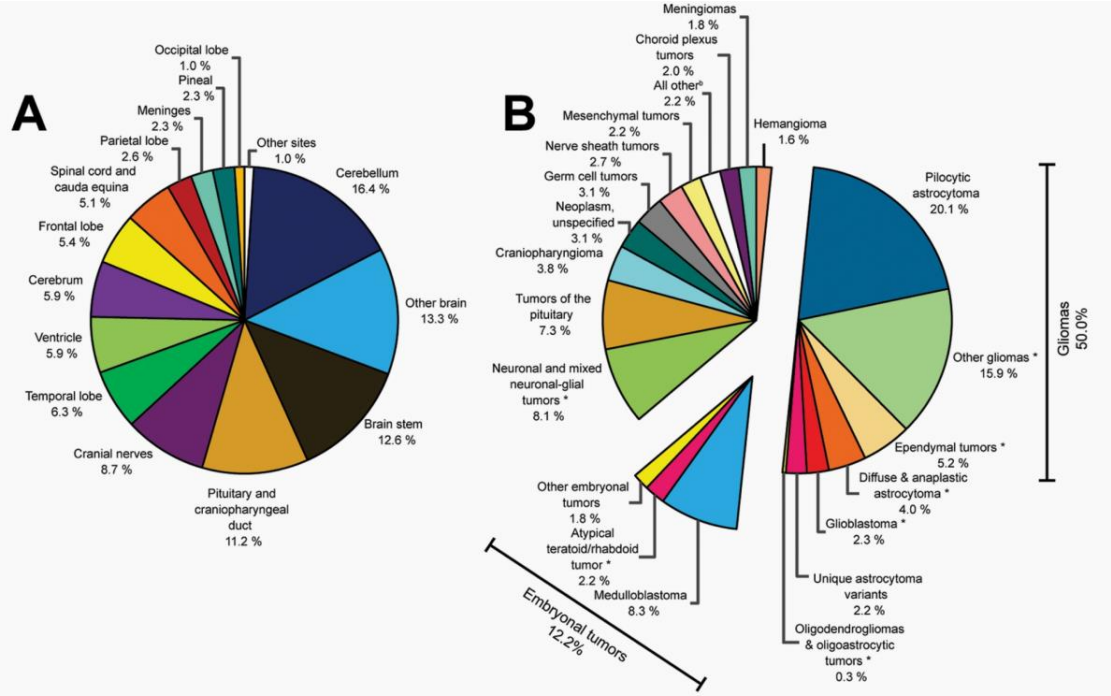

* All or some of the codes used to define this histopathology are included in the CBTRUS definition of gliomas, including ICD-O-3 histopathology codes 9380-9384 and, 9391-9460 (Table 2).
a. Percentages may not add up to 100% due to rounding.
b. Includes glioblastoma, pilocytic astrocytoma, unique astrocytoma variants, ependymal tumors, choroid plexus tumors, choroid plexus tumors, tumors of the pineal region, tumors of the pineal region, nerve sheath tumors, other tumors of cranial and spinal nerves, other tumors of cranial and spinal nerves, meningiomas, mesenchymal tumors, primary melanocytic lesions, primary melanocytic lesions, lymphoma, lymphoma, other hematopoietic neoplasms, other hematopoietic neoplasms, germ cell tumors, tumors of the pituitary, craniopharyngioma, hemangioma, neoplasm, unspecified, all other, all other (Table 2).
Data Source: CBTRUS Statistical Report: US Cancer Statistics – NPCR and SEER, 2017–2021
Abbreviations: CBTRUS, Central Brain Tumor Registry of the United States; NPCR, National Program of Cancer Registries; SEER, Surveillance, Epidemiology, and End Results Program.

Figure 1.1.: Distribution of primary CNS and brain tumors in children (age 0-14 years); Price et al. (2024) made available with Copyright Clearance Center's RightsLink service

Incorporation of molecular characteristics to classify pediatric brain tumors was a significant step in the classification of central nervous system (CNS) tumors by the World

Health Organization (WHO) in 2021 (Louis et al., 2021). The consideration of molecular biomarkers is most important for proper diagnosis and prognosis, for the choice of appropriate treatment, and for inclusion in relevant clinical trials (Price et al., 2024).
Grades 1 to 4 are the categories for brain tumors according to the WHO classification. Brain tumors with grades 1 and 2 are considered as low-grade lesions, and grades 3 and 4 belong to the group of high-grade lesions (NHS inform, 2024; Louis et al., 2021). In children, gliomas, including low-grade as well as high-grade lesions, are the most frequent malignant subgroup of brain cancer (Figure 1.1). Gliomas develop from glial cells, which are supportive cells in the brain and spinal cord, or from neural stem/progenitor cells that give rise to glial cells. These tumors arise within the supportive tissue of the CNS (National Cancer Institute, 2024).

Pediatric high-grade gliomas

Pediatric high-grade gliomas (HGGs) account for around 10% of all CNS tumors (Ostrom et al., 2022). Around 40% of all brain tumor-associated deaths in children are made up by this kind of tumor. Despite multimodal treatment, 28.4% of children survive five years after diagnosis (Ostrom et al., 2015).
Based on molecular diagnostics including Next Generation Sequencing (NGS) and DNA methylation analyses, pediatric HGGs got reclassified and divided into refined subgroups (Louis et al., 2021). These subgroups differ in molecular and clinical traits, such as the tumor location, molecular characteristics (e.g. genetic alterations, DNA methylation changes, chromosomal aberrations), and survival outcomes. Subgroups of HGGs defined by genome-wide methylation profiles are characterized by conserved epigenetic characteristics. Variants in histone H3.1 and H3.3, precisely mutations in *H3F3A* and *HIST1H3B*, are on position K27 and G34 (Khuong-Quang et al., 2012). Tumors with mutations in G34, IDH (isocitrate dehydrogenase), and *BRAF V600E* are more likely found in the cerebral hemispheres (Figure 1.2).

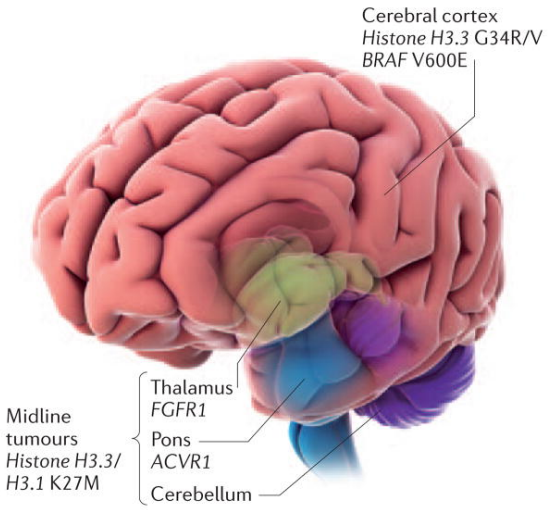

Figure 1.2.: Subgroups of high-grade gliomas and their location.
Illustration showing the predominant tumor location in different HGG subgroups. (Pollack et al., 2019); made available under a Creative Commons or similar license by PubMed Central (PMC)

Tumors of the K27M-altered subgroup (diffuse intrinsic pontine gliomas (DIPG) and HGGs of the thalamus) are predominantly located in the midline section of the brain. K27M alterations lead to loss of the trimethylation in lysine at position 27 which interacts with the polycomb repressive complex (PRC2). This interaction leads to suppression of transcription of target genes which has an impact on cell development and regulation (Castel et al., 2015).

The patient age at diagnosis and survival times vary between the different subgroups of HGG (Figure 1.3). Tumors harboring a mutation in G34 or IDH are indicated in adolescents and the overall survival (OS) time under treatment is around 6 years. Children with *BRAF*-mutated HGG survive up to 8 years. Tumors with K27 mutation are mostly diagnosed in children between three and ten years who survive around 24 months (Jones et al., 2017).

Standard therapy for pediatric HGG is maximal gross resection and radiation therapy. This leads to the best OS rate. Additional chemotherapy increases OS and event-free

survival (for details see chapter 1.1) still leaving affected patients with a rather poor prognosis. Therefore, novel improved therapies are urgently needed (Guidi et al., 2021).

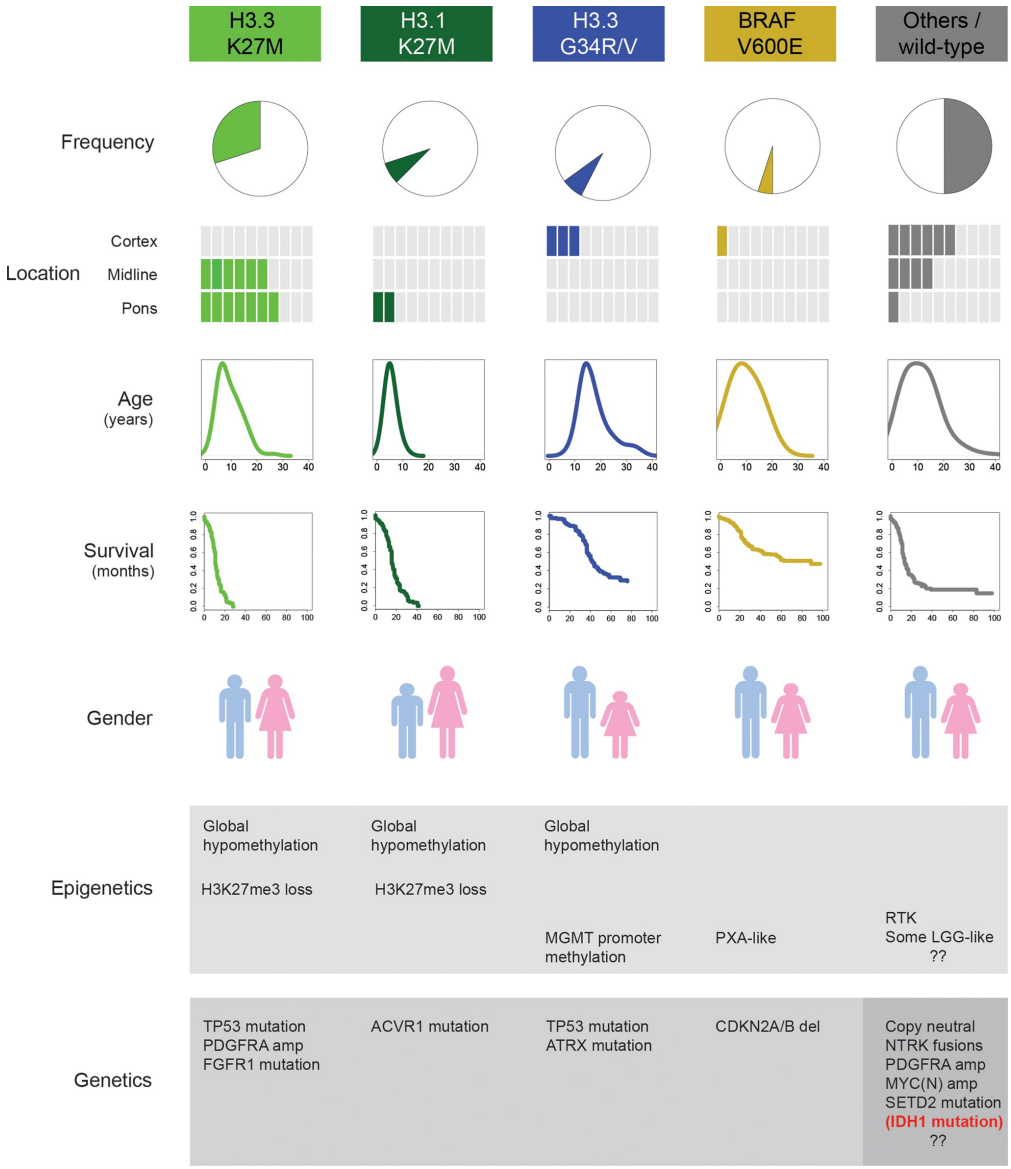

Figure 1.3.: Summary of HGG subgroups showing the frequency of occurrence, predominant tumor location, age of diagnosis, survival rate under treatment, gender distribution, and concomitant mutations. (Jones et al., 2017); made available under the Creative Commons CC-BY-NC license with Copyright Clearance Center's RightsLink service

BRAF-V600E mutation

V-raf murine viral oncogene homolog B1, short *BRAF*, is a serine/threonine protein kinase and is an important mediator in the mitogen-activated protein kinase (MAPK) pathway. When growth factors bind to receptor tyrosine kinases (RTKs), *BRAF* is itself activated by the small GTPase (guanosine triphosphate) RAS (rat sarcoma protein) (Figure 1.4) (Capogiri et al., 2023). The BRAF kinase activates and phosphorylates downstream mediator MEK (MAPK kinase), which activates ERK (extracellular-signal-regulated kinase). ERK itself translocates into the nucleus where it acts as a transcription factor, which regulates cell proliferation, differentiation, growth, and survival (Smalley and Smalley, 2018).

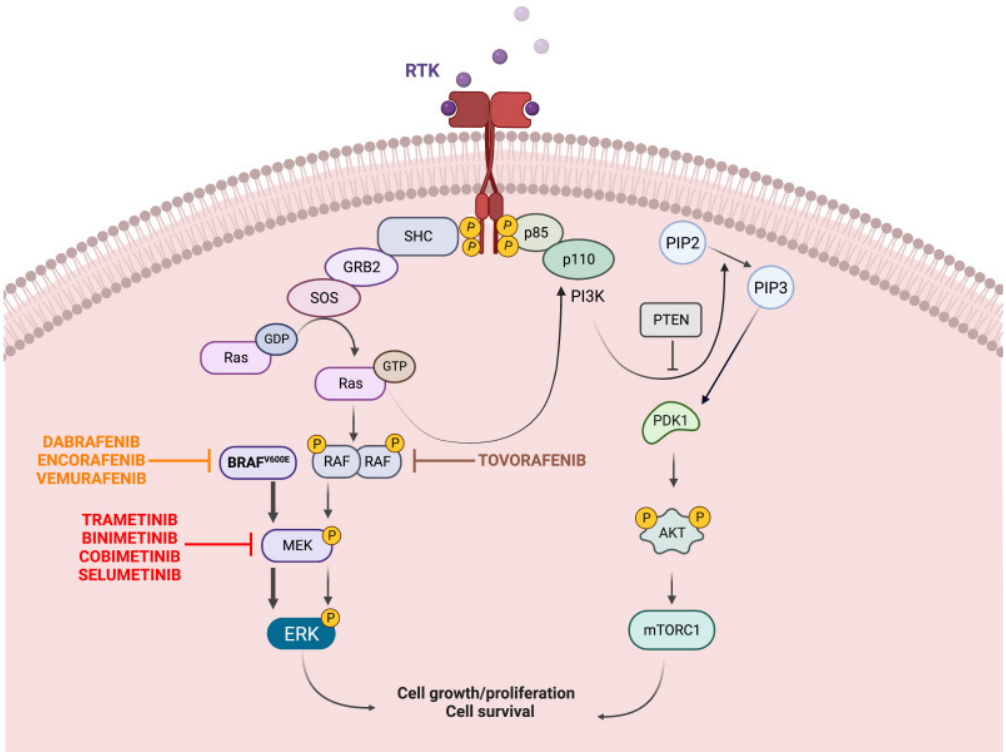

Figure 1.4.: RAS/RAF/MEK/MAPK signaling pathway and PI3K/AKT/mTOR survival pathway with *BRAF V600E* mutation, and BRAF and MEK inhibitors shown. (Capogiri et al., 2023); made available under a Creative Commons or similar license by PubMed Central (PMC)

BRAF is one of the most frequently altered genes and oncogenic driver in diverse human cancers including melanoma, papillary thyroid carcinoma, colorectal cancer, non-small cell lung cancer as well as both LGG (around 20%) and HGG (5-15%) (Capogiri et al., 2023). Three classes of over 30 *BRAF* alterations in human cancer have been identified based on their dependency on RAS, their status of dimerization, and their activity of the kinase. All alterations cause activation of the MAPK pathway (Kowalewski et al., 2020).

- With mutations of class I, BRAF is active as a monomer and activation by upstream RAS resulting in RAS-independent MAPK signaling. This class is the most common in CNS tumors as well as melanoma, non-small cell lung cancer, and many more. The most common mutation is a point mutation on codon 600, where valine (V) is substituted with glutamic acid (E) (V600E). This mutation leads to constitutive *BRAF* activation and therefore oncogenesis (Yao et al., 2015).

- Class II alterations characterize constitutively active dimers. The result of class II alterations is higher activity in MAPK signaling because of increased dimerization of *BRAF* with RAS-independent *BRAF* activation. The most common fusion in this class is between *KIAA1549* and *BRAF* (Yao et al., 2015).

- Class III *BRAF* alterations represent a third class of *BRAF* mutants that have impaired kinase activity or are kinase-dead. These mutants rely on RAS-dependent activation of signaling and are sensitive to ERK-mediated feedback, making them distinct from other *BRAF* mutation classes in their response to targeted therapies (Yao et al., 2017).

Standard of care and targeted therapies

Standard of care

For HGG, the standard of care is surgery followed by radiotherapy and chemotherapy using temozolomide (TMZ). Surgical resection and the extent of resection are very important

for the OS. The aim of surgery is to remove as much tumor tissue as possible, without negatively impacting the total patient performance. Notably, HGGs are characterized by highly infiltrative growth, hampering complete resection (Chaichana et al., 2014). Therefore radiation therapy is applied as a next step following surgery. The mode of action of radiotherapy is to kill rapidly dividing tumor cells by introducing nonspecific breaks in the DNA strands (Hingorani et al., 2012). In children, radiotherapy is usually applied locally. Simultaneously, TMZ is given orally in six cycles each containing 5 days. TMZ is a nonspecific alkylating agent that leads to apoptosis of the remaining tumor cells. It methylates at position O^6 of guanine which leads to mismatch repair causing endless cycles of repair and breakage in DNA strands (Brock et al., 1998).

In most cases, the standard of care results in progression of HGGs, so other therapeutic approaches are needed. Improvement in molecular tumor characterization helped with finding possible therapeutic targets, such as *BRAF*. Developing and testing diverse BRAF inhibitors binding the mutated protein was crucial for prolonging patients' lives (Rosenberg et al., 2022). Figure 1.5 shows a timeline of several developed BRAF inhibitors that were partially approved by the US Food and Drug Administration (FDA).

First generation inhibitors

In 1999, before the identification of *BRAF* mutations, the *first generation* of *BRAF*-targeting inhibitor ZM336372 had been developed, since *BRAF* had already been acknowledged as cancer target. These *first-generation* inhibitors were small-molecule ATP-competitive agents targeting both *CRAF* and *BRAF* in tumors (Hall-Jackson et al., 1999; Capogiri et al., 2023). By imitating the structure of ATP, these inhibitors compete with ATP for the catalytic site in *BRAF*/*CRAF*, therefore inhibiting the kinase activity of these molecules (Polier et al., 2013). Sorafenib (Nexavar, BAY43-9006) is the only first-generation inhibitor approved by the FDA. Surprisingly, Sorafenib had no significant anti-tumor effects in tumors harboring the *BRAF V600E* mutation, and also *BRAF*-fused

tumors showed accelerated growth on therapy (Tabernero et al., 2013; Karajannis et al., 2014). The so-called BRAF paradox leads to an increased MAPK signaling while BRAF inhibition when RAS is mutated or upstream activated. This paradoxically hyperactivates the MAPK pathway and is particularly observed with first generation inhibitors (Oberholzer et al., 2012).

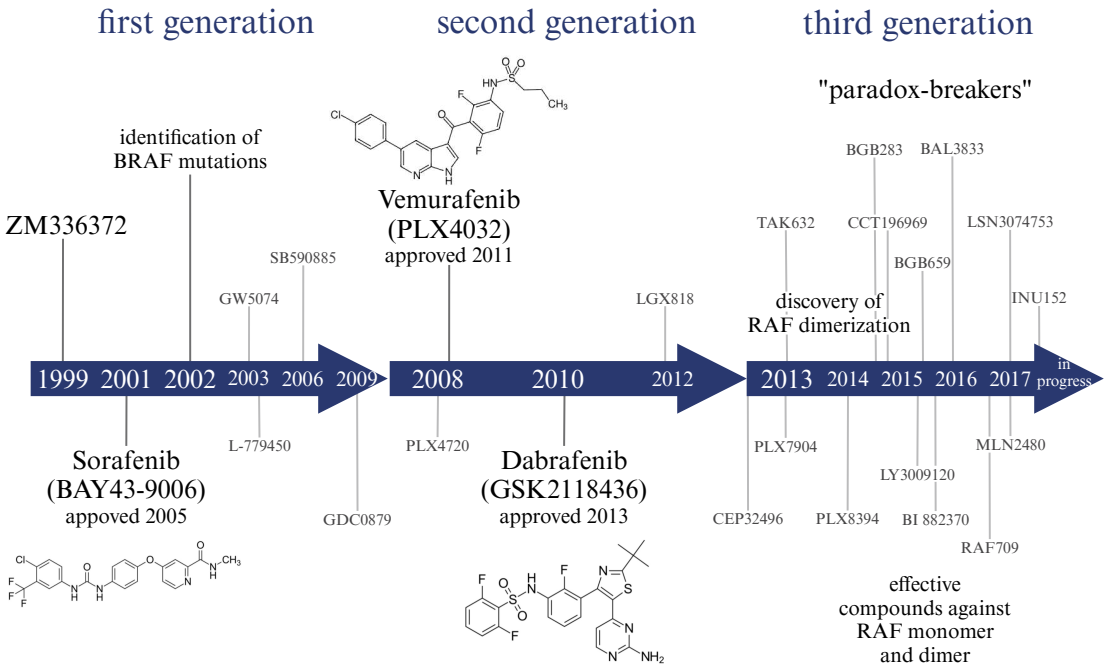

Figure 1.5.: Development of BRAF inhibitors over time, year of approval by the FDA, and to which generation they belong.; Created in BioRender.com

Second generation inhibitors

The identification of *BRAF* mutations in 2002, especially *BRAF V600E*, motivated the development of new compounds targeting mainly *BRAF V600E* (*second generation* BRAF inhibitors) (Davies et al., 2002). Plexxikon developed the second generation inhibitor vemurafenib (PLX4032) for binding the ATP-binding site of the V600E mutated BRAF kinase, leading to *BRAF* inhibition. The inhibition of mutated *BRAF* causes repression of ERK phosphorylation resulting in reduced cell proliferation and cell death induction (Joseph et al., 2010). Vemurafenib is the first selective inhibitor against *BRAF* tested

on patients with *BRAF V600E*-mutated melanoma. It got approved in 2011 by FDA (Sosman et al., 2012). Another inhibitor of the second generation is dabrafenib which is used for treating metastatic or unresectable solid tumors. It also binds to *BRAF V600E* to stop the downstream signaling of the MAPK pathway (Robert et al., 2015). Dabrafenib leads to a better response in melanoma than vemurafenib. Dabrafenib has a better blood-brain barrier (BBB) penetration and a significantly smaller half-maximal inhibitory concentration (IC50) value compared to vemurafenib and is, therefore, the drug of choice. (Mittapalli et al., 2013).

Third generation inhibitors

Third generation RAF inhibitors have been developed after discovering RAF dimerization. There are two types of these inhibitors:

- There are effective inhibiting compounds for dimeric or monomeric forms of RAF. This is expected to reduce resistance against inhibitors due to RAF dimerization (Koumaki et al., 2021).
- The so-called pan-RAF inhibitors are "paradox breakers". These prevent paradoxical activation of the MAPK pathway (Vakana et al., 2017).

Although these RAF inhibitors prolong patients' lives, they have limits. In most cases, the tumor develops resistance against the drugs and recurs. To improve the response and reduce the chance of resistance, combination therapy with MEK inhibitors was tested and showed better efficacy (Long et al., 2014). The MEK 1/2 inhibitor selumetinib (AZD6244, ARRY-142886, Koselugo) is a small-molecule, ATP-noncompetitive compound with FDA-approval for specific indications, such as neurofibromatosis 1 (NF1). It promotes apoptosis and inhibits cell proliferation by targeting MEK1/2 kinase. ATP-noncompetitive inhibitors bind to an allosteric site outside the ATP-binding pocket, stabilizing the kinase in an inactive conformation. This prevents MEK phosphorylation by RAF and disrupts

key regulatory mechanisms necessary for kinase activation (Wu and Park, 2015).

Resistance mechanisms

Combination therapy of BRAF inhibitors with MEK inhibitors shows better results than BRAF inhibitors alone (Long et al., 2014). Despite the combination of all types of therapy like surgery, radiotherapy, chemotherapy, and targeted therapy, resistance mechanisms against targeted therapy are still a big challenge (Figure 1.6) (Sasame et al., 2022). While several resistance mechanisms have been identified in other cancers, studies in pediatric HGG remain limited, leaving a substantial gap in the field. Patients continue to develop resistance, highlighting the urgent need for further research to uncover strategies that can enhance survival and overcome these barriers.

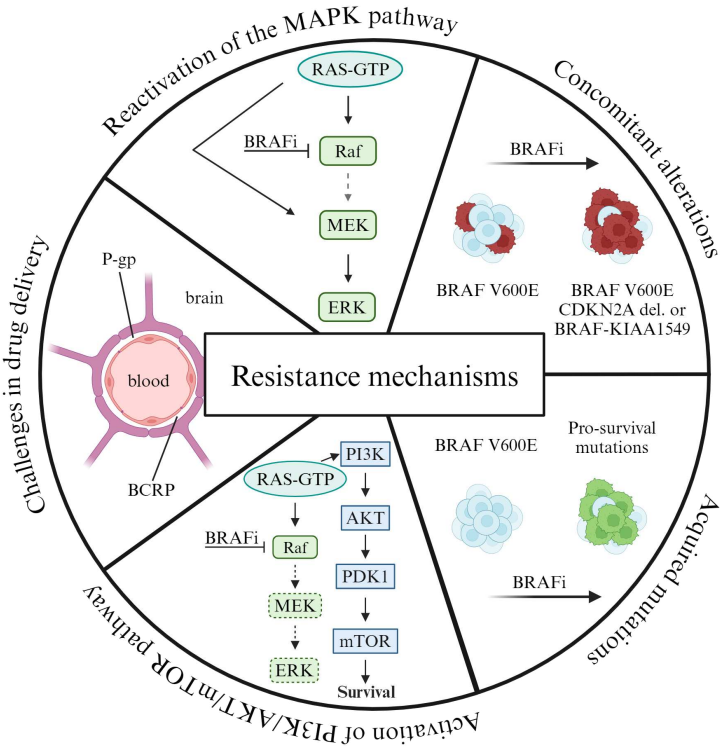

Figure 1.6.: Outline of resistance mechanisms of BRAFV600E-mutated high-grade gliomas towards BRAF inhibitors.; Created in BioRender.com

Reactivation of the RAS/RAF/MEK/ERK pathway

Reactivation of the MAPK pathway is the reason for around 80% of all resistance mechanisms against *BRAF*-targeting drugs in tumors with *BRAF V600E* mutation. (Capogiri et al., 2023). Some mechanisms for reactivation are upregulated RTKs like EGFR, PDGF-β, and IGF1R, secondary mutations in the RAS/RAF/MEK/ERK pathway, or alternative splicing of *BRAF* (Capogiri et al., 2023; Lehmann et al., 2022). Secondary mutations are induced and acquired after therapy in targeted oncogenes with mutations (Wang et al., 2018).

Concomitant alterations

Another reason why therapy with BRAF inhibitors fails is the presence of concomitant alterations in tumor cells like deletion of *CDKN2A*.

The BRAF-KIAA1549 fusion is another concomitant alteration that can occur with *BRAF V600E* which leads to rapid progression under treatment (Capogiri et al., 2023).

Acquired mutations

Development of new mutations leads to relapse of the tumor after a good initial response to BRAF inhibitors alone or in combination therapy with MEK inhibitors (Capogiri et al., 2023).

Activation of PI3K/AKT/mTOR pathway

Another identified reason for drug resistance is the presence of interconnections and redundancies between the MAPK pathway and other signaling pathways, a phenomenon referred to as pathway crosstalk (Capogiri et al., 2023).

Increased activation of AKT and mutations in *PIK3C2G* are responsible for activation of the PI3K/AKT/mTOR pathway (Lehmann et al., 2022). The functions of *PIK3C2G* are implicated in cell functions like survival, growth, and proliferation. Loss of the

negative regulator *PTEN* is common in tumors and leads to increased signaling of the PI3K/AKT/mTOR pathway and decreased apoptosis during therapy with BRAF inhibitors (Schreck et al., 2021).

Challenges in drug delivery

Crossing the blood-brain and blood-tumor barrier is important for drugs to reach the tumor. Most of the available drugs are not capable of crossing the BBB, which limits the effectiveness of the treatment. Efflux of inhibitors like dabrafenib and vemurafenib from tumor cells is a result of the higher expression of the P-glycoprotein (*P-gp*) and the breast cancer resistance protein (*BCRP*) at the cell membrane and represents one common resistance mechanism (Capogiri et al., 2023).

1.2. Identification of the research problem

HGGs are among the most aggressive pediatric brain cancers in children. A subset of (pediatric) HGG, thyroid cancers, malignant melanomas, and non-small cell lung cancers amongst other cancer entities harbors a characteristic mutation at V600E in the *BRAF* gene. This mutation is targetable with the small-molecule inhibitor dabrafenib, which is already in clinical use. Previous studies have shown that HGGs in children harboring this mutation become resistant against dabrafenib after a few months of treatment leaving children with limited prognoses and treatment options. Therefore, we developed the following research questions:

Research questions

How does global gene expression change in BRAF inhibitor-resistant models? (RNA Sequencing, Expression Arrays)

Which mutations arise or get lost in BRAF inhibitor-resistant samples? (Whole Exome Sequencing)

Which chromosomal aberrations (focal and global amplifications or deletions and loss of heterozygosity) occur in BRAF inhibitor-resistant samples? (Array Comparative Genomic Hybridization, Whole Exome Sequencing)

Are the identified resistant mechanisms in pediatric high-grade gliomas in alignment with identified resistance mechanisms towards BRAF inhibitors in other cancers, like thyroid cancer, malignant melanoma, and low-grade gliomas? (all high-throughput methods)

Can we leverage high-throughput drug screens to identify alternative treatment targets within BRAF inhibitor-resistant cell cultures and how do these potential targets correlate with the genomics and transcriptomics of the resistant subline? (all high-throughput methods and drug screens)

Aims

My goals for this project were (1) learning to work with and integrate different data types (whole-exome sequencing, RNA sequencing, expression arrays, Comparative Genomic Hybridization Arrays, high-throughput drug screens) and (2) analyze their relationship in the background of cancer research. By answering the research question outlined above, I aimed to (3) identify mutations or genetic alterations that could contribute to resistance development in high-grade gliomas in children.

2. Materials and Methods

2.1. Ethical considerations and human subjects

Tumor tissues used to establish patient-derived cell models were obtained from patients treated at Vienna General Hospital. The patient's legal representative signed informed consent for the use of tumor material. The use of tumor material was confirmed by the ethics committee of the Medical University of Vienna, Austria under the internal review board number 1244/2016. Patients were deidentified and cell models run under identification numbers with the prefix Vienna Brain Tumor (VBT).

2.2. Cell models

Cell models from the tumor of a pediatric patient with HGG, who was treated at the Medical University of Vienna, were established. In specific, data of three cell models are included in this thesis: one from the primary treatment-naive tumor (VBT92, grade III anaplastic pleomorphic xanthoastrocytoma), one from the dabrafenib therapy-refractory recurrence (VBT125, grade IV gliosarcoma) (Gabler et al., 2019), and one which was propagated towards increased dabrafenib resistance *in vitro* (VBT125Dabra) by continuous exposure to increasing drug concentrations. The final dabrafenib concentration reached was 10 μM. Whole exome sequencing, array Comparative Genomic Hybridization, bulk RNA sequencing, and mRNA expression arrays of these models were performed prior to the start of this thesis project, and data were analyzed in the course of this master's

project.

2.3. mRNA expression arrays

Principle

Two-color microarrays are a robust way to study gene expression profiles using hybridization. Since samples are stained with two colors, two samples can be analyzed within one microarray. Microarrays are characterized by bound oligonucleotide sequences which are complementary to complementary RNA (cRNA). Upon RNA isolation from the used tissues or cells, the first experimental step is to transcribe the mRNA into complementary DNA (cDNA) which is further converted to cRNA. One sample gets marked with the fluorescent dye cyanine-based Cy3 (green) and the other with Cy5 (red). The next step is to hybridize the fluorescent samples onto probes, which are fixed on a coated glass slide. These probes correspond to a gene transcript. Gene expression is computed with statistical analysis of the fluorescent signals. It is recommended to perform two-color arrays in at least two biological and technical replicates to improve the robustness and stability of results (Knapen et al., 2009)

Experimental specification

Isolation of RNA and Whole Genome Gene Expression Arrays:
RNA was isolated using the RNeasy Mini Kit (Qiagen). Quantity and integrity of the RNA samples were checked on an Agilent 2100 Bioanalyzer, and only samples with an RNA integrity number (RIN) > 8 were included for microarray experiments. Gene expression arrays were performed using 4x44K whole genome oligonucleotide-based gene expression arrays (Agilent). Labeling and hybridization procedures were performed according to the instructions provided by Agilent using the QuickAmp Labeling Kit and the Two Color Microarray-Based Gene Expression Analysis Protocol.

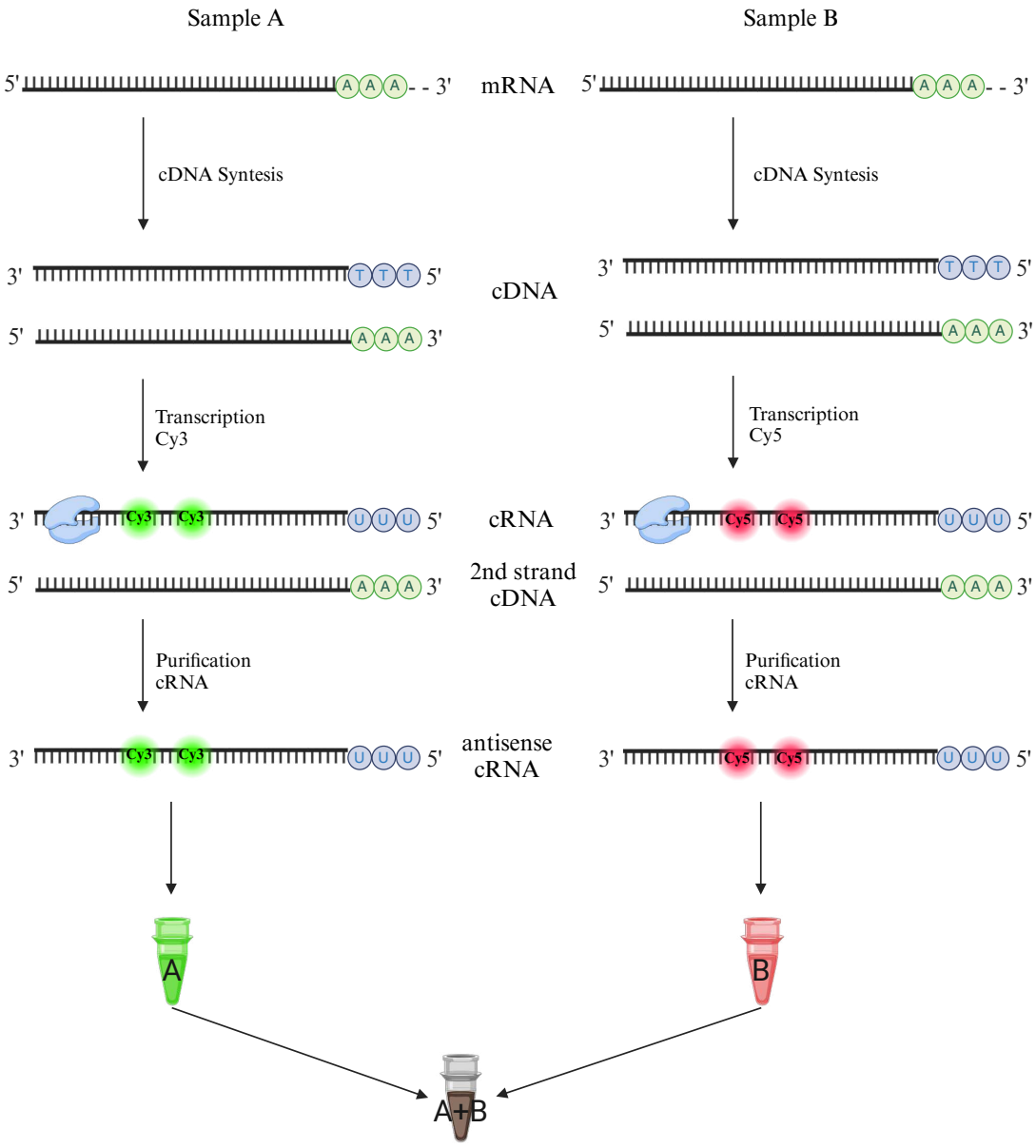

Figure 2.1.: Schematic illustration of processing mRNA for Agilent two-color microarrays. Created in BioRender.com

Figure 2.1 provides an overview of the labeling and hybridization procedure. Shortly, in a first step 500ng of RNA were converted into cDNA using a T7 promoter primer. In a second labeling and amplification step, cDNA was converted into Cy3- or Cy5-labeled

cRNA (two color experiments). After purification of labeled cRNAs with the RNeasy Mini Kit (Qiagen), 825ng Cy3- and 825ng Cy5-labeled cRNA were mixed and, together with Blocking Agens and Fragmentation Buffer, incubated for 30 min at 60°C (heat fragmentation). Afterwards, 2xGE Hybridization Buffer was added to each sample, a gasket slide was put into the microarray chamber, and the sample mixtures were pipetted onto the gasket slide. The microarray slide was then positioned face-down on samples and gasket slide and the hybridization chamber was closed. Hybridization was carried out for 17 h at 65°C in a hybridization oven (Agilent). Next, slides were washed according to the protocol and scanned with a G2600D Microarray Scanner (Agilent). Feature extraction was carried out using the Feature Extraction software (version 11.5.1.1).

Implementation

Raw data from each condition was extracted and preprocessed in R v4.4.1 using the *limma* package v3.58.1. Precisely, background correction was performed, and dual-colour array data was normalized using the *limma* functions *backgroundCorrect()* (method = "normexp"), *normalizeWithinArrays()* (method = "loess") and *normalizeBetweenArrays()* (method = "Aquantile"). The *hgug4112a.db* R package v3.2.3 was used to create the features annotations. In the case of multiple probes per gene, the data was averaged using the *avereps() limma* function. $\log_2$ fold changes (logFC) were calculated between contrasts of interest with the *limma* package, gene set enrichment analysis from the *clusterProfiler* package v4.10.0 and gene set variation analysis from the *GSVA* package v1.50.2 were performed.

2.4. RNA sequencing

Principle

RNA sequencing (RNA seq) is a method to analyze the quantity of a transcriptome. Besides the global gene expression profiles of samples, allele-specific expression, and different alternative splicing events can be detected (Ura et al., 2022). High-quality RNA is isolated from samples and subsequently transformed into cDNA. Following stringent quality control, the prepared cDNA library is sequenced with next-generation sequencing (NGS) (Kukurba and Montgomery, 2015; Mackenzie, 2018). These reads from the NGS are saved in FASTQ-files, get aligned to a reference genome and gene expression is computed.

Implementation

cDNA library was prepared with *NEB Ultra Directional RNA Library Prep Kit (dUTP method)* and sequenced with *Illumina paired-end sequencing protocol*. As reference genome `"https://genome-idx.s3.amazonaws.com/hisat/grch38_genome.tar.gz"` was used for the alignment.

The resulting counts files were pre-processed and used for the features annotations created with the *org.Hs.eg.db* R package v3.2.3. The data frame containing the counts was converted to a Digital Gene Expression data list with *DGEList()* and then "counts per million" were calculated with *cpm()*, both functions from the *edgeR* v4.0.12. package. To avoid zero counts, +1 was added and *log2()* from *base* v4.3.2 was used to compute the $\log_2$ values for the calculation of the logFC between contrasts of interest. Gene set enrichment analysis using the *clusterProfiler* package v4.10.0 and gene set variation analysis from the *GSVA* package v1.50.2 were performed.

2.5. Limma package

Principle

Limma is a package of the R or Bioconductor software and stands for "linear models for microarray data". This package analyzes the outcome of experiments for gene expression from different technologies like microarrays, RNA seq, or high-throughput polymerase chain reaction (PCR). Even if the experiments have complex designs, their data can be read, normalized, and explored with limma. The aim is to fit a linear model to the data of the expression experiments for each gene (Ritchie et al., 2015; Smyth, 2005).
The first step is reading data, for two-colour microarrays these are the images of the arrays with foreground and background intensities included. For RNA seq, the data consists of a matrix with the count reads which is converted in a DGEList. Background correction cancels out these background signals of microarrays. The next step is to filter for batch effects that may occur due to poor arrays. The correlation is computed with the averaged, filtered, and annotated array data between the hybridized channels of one two-color microarray. The *lmscFit() limma* function fits a linear model to the array data with this correlation value to analyze the data as if it is data of a one-channel microarray. This method is called separate channel analysis. The *lmFit limma* function, which was originally implemented for microarrays, can also be used for RNA seq data and fits a distinct model to the expression values for every gene. Then logFC are calculated, t-statistics estimated with the contrast matrix, and the linear model fitted data for the contrasts of interest. To reduce the gap between the estimated variances of the genes and the known variance, the empirical Bayes can be used. This lowers the amount of false positives for genes. The top-ranked genes are then extracted and saved in a new data frame (Ritchie et al., 2015).

Implementation

Expression arrays

Data was read in with *readTargets()* and *read.maimages()* from the *limma* package v3.58.1. Background correction and normalization were performed with the functions *backgroundCorrect()* (method = "normexp"), *normalizeWithinArrays()* (method = "loess") and *normalizeBetweenArrays()* (method = "Aquantile"). For annotation features the *hgug4112a.db* R package v3.2.3 was used. The data frame of the targets file was converted to a data frame with one row per entry in the dyes columns with the *limma* function *targetA2C()*. Then the unique values of this target column with *limmas unique()* and *factor()*, and the column itself created a design matrix of the experiment with *model.matrix()* function of *stats* package v4.3.2. With the *makeContrasts() limma* function and the design matrix, a contrast matrix with the contrasts of interest was implemented. The averaged (with *avereps()*), filtered, and annotated array data and the design matrix were input for the *limma* function *intraspotCorrelation()*. The *lmscFit()*, the *contrasts.fit()* and the *eBayes()* functions from the *limma* package were used to fit a model to the data and to get more reliable and stable values. The top-ranked genes were extracted with the *limma* function *topTable()* with the Benjamini-Hochberg ("BH") method.

RNA sequencing

The RNA seq data was read with *read.delim()* function from the *utils* package v4.3.2. Feature annotations were made with the *org.Hs.eg.db* R package v3.2.3 and the counts data was averaged with the *dplyr* v1.1.4 function *summarize_ all(mean)*. This data frame was converted into a DGEList, which created the design matrix with its row names with the *model.matrix()* function of *stats* package v4.3.2. A contrast matrix was generated with the function *makeContrasts()* of the *limma* package v3.58.1. The calculated $\log_2$ values of the counts per million and the design matrix were the input of the *lmFit limma* function to fit a linear model to the data. The *limma* functions *contrasts.fit()*, *eBayes()*,

and *topTable()* with adjust = "BH" were used to compute stable standard errors and put the top-ranked genes in a data frame like for expression arrays.

2.6. GSEA - Gene Set Enrichment Analysis

Principle

Gene set enrichment analysis (GSEA) is a tool to analyze and compare gene expression data between two samples or groups of samples. It can be used to interpret the differential gene expression between drug-sensitive and drug-resistant tumors in terms of genes' functions. Such as, genes are summarized to gene sets based on a common feature such as their biological function. GSEA may use any gene sets, custom-designed or publicly available predefined gene sets, which are saved in Gene Matrix Transposed (GMT) files. Publicly available files can be downloaded from the *Molecular Signature Database, MSigDB* website. The genes are ranked by their gene expression values and saved in a gene list. The aim of GSEA is to show if the genes in a gene set are found mostly at the top or the bottom of the ranked list. This is done in 3 steps: first, the enrichment score (ES) is calculated. The ES is the maximum deviation from zero. It indicates the extent to which the genes are located at the top or the bottom of the list. This is calculated with an increase if the gene is in the gene set and with a decrease if not. The second step is to rate the significance of the ES, called p-value. The p-value is calculated with an empirical phenotype-based permutation test procedure. The last step is to adjust the values for comparison of the gene sets. The ES gets normalized by including the size of the gene set (Subramanian et al., 2005). To adjust the p-value, the Benjamini-Hochberg ("BH") method is used. The false discovery rate is computed. The previously calculated p-values are sorted and ranked. A critical value is calculated by the false discovery rate times the rank of the current p-value divided by the total number of p-values. Gene sets with an adjusted p-value smaller than the critical value are considered significant (Reiner et al., 2003).

Implementation

At first, a gene list with the previously calculated logFC values and the annotated gene names was generated with the *deframe()* function from the *tibble* package v3.2.1. This list needs to be sorted by a decreasing order for the GSEA. For this project, GMT files KEGG and REACTOME from the section C2, and BP (biological process), CC (cellular component), and MF (molecular function) from the C5 section were used (version 2023.2.Hs.symbols). The C2 section was predefined by online databases for pathways and by biomedical literature, and the C5 by ontology resources. *GSEA()* from *clusterProfiler* package v4.10.0 was used for the analysis with the following non-default settings: pvalueCutoff = 1, minGSSize = 15, eps = 0.

2.7. GSVA - Gene Set Variation Analysis

Principle

Gene set variation analysis (GSVA) is a method for estimating gene set variation between samples independent of the defined classes, such as "therapy-resistant" and "therapy-sensitive". The input is a matrix with normalized expression values of expression arrays or RNA seq and GMT files with predefined gene sets. At first, the algorithm uses the sample population distribution to estimate the gene expression levels of a sample. A gene expression-level statistic is computed for a distinction of the expression profiles and genes are ranked for each sample. Sample-wise ES are used for expression-level statistics for gene sets. With the expression value matrix and the gene set files, the maximum deviation ES and the normalized enrichment score (NES) are calculated. One of these ES is the output for pathways in each gene set and sample (Hänzelmann et al., 2013).

Implementation

The previously calculated fit coefficients with the annotated gene symbols were used for an expression matrix. The GMT files KEGG and REACTOME from the section C2 and BP, CC, and MF from the C5 section on the *MSigDB* website were part of the input. A gene list was generated with the genes and terms of these GMT files. The GSVA was executed with the *gsva()* function from the *GSVA* package v1.50.2 with this expression array, this gene list and these non-default options: min.sz = 1, max.sz = 1000, mx.diff = FALSE.

2.8. Whole exome sequencing

Principle

Whole exome sequencing (WES) is a tool to identify copy number variations (CNVs) and single nucleotide variants (SNVs) in protein-encoding genes (Bartha and Győrffy, 2019). First, high-quality RNA-free genomic DNA (gDNA) is extracted. gDNA is fragmented mechanically or biologically (Seaby et al., 2016). The ends of fragments can be unequally long on the double strand. To even this out, either the missing base pairs are added or the additional base pairs are removed. Adaptors are necessary to start the reading process. For these, an additional single adenine (A) nucleotide is needed at one strand. Adaptors have an additional thymine (T) nucleotide which binds to the additional A (Twist Bioscience, 2018a). Then exonic regions get enriched. Illumina uses hybridization for targeted enrichment. Complementary sequences of DNA to specific genomic regions of interest are designed. These sequences, called probes, are mixed with the genomic sample. The mixture is heated to part the gDNA, then cooled down to reactivate the binding process where the probes bind with the complementary strands of the gDNA. Magnetic beads binding to the probes are added and a magnet pulls out the bound exome DNA (Twist Bioscience, 2018b). This bound exome DNA is washed over flow cells. On

these cells, complementary matches of the adapters on the single-strand DNA are fixed and bind to the adapters. Nucleotides are each labeled with a unique fluorescent color and added to the flow cells. This requires four circles because each nucleotide needs to be added separately. The nucleotides bind to the single-strand DNA, and the sequencer images the fluorescent signal. The results of parallel sequencing of the developed library are short paired-end reads. These reads are saved in a FASTQ file (Twist Bioscience, 2018c). These files get aligned to a human reference genome and a variant caller is used to detect variants, which are then annotated and filtered to identify genes (Seaby et al., 2016).

Implementation

The resulting .bam files were converted to FASTQ files with *bedtools* v2.31.1 and the two lanes got merged. These two FASTQ files were mapped with *bwa mem* function of *bwa* v0.7.15 and aligned to *human_g1k_v37bwa.mem* as a reference genome. *samblaster* v0.1.26 was used to delete duplicates and to create a file containing the unmapped reads, and *sambamba* v0.7.1 to sort the reads. *BaseRecalibrator* and *PrintReads* from the *Genome Analysis Toolkit* (GATK) v3.8 package updated the alignment data with adjusted base quality scores. *HaplotypeCaller* and *VariantFiltration* from the *GATK* package v3.8. are functions for variant calling and filtering. Then coverage was calculated with *bedtools* v.2.31.1, and somatic variations, especially tumor mutations, were identified. These were filtered based on function-specific quality scores with *GATK* v4.5.0.0 functions *Mutect2* and *FilterMutectCalls*. This whole process is illustrated in figure 2.2

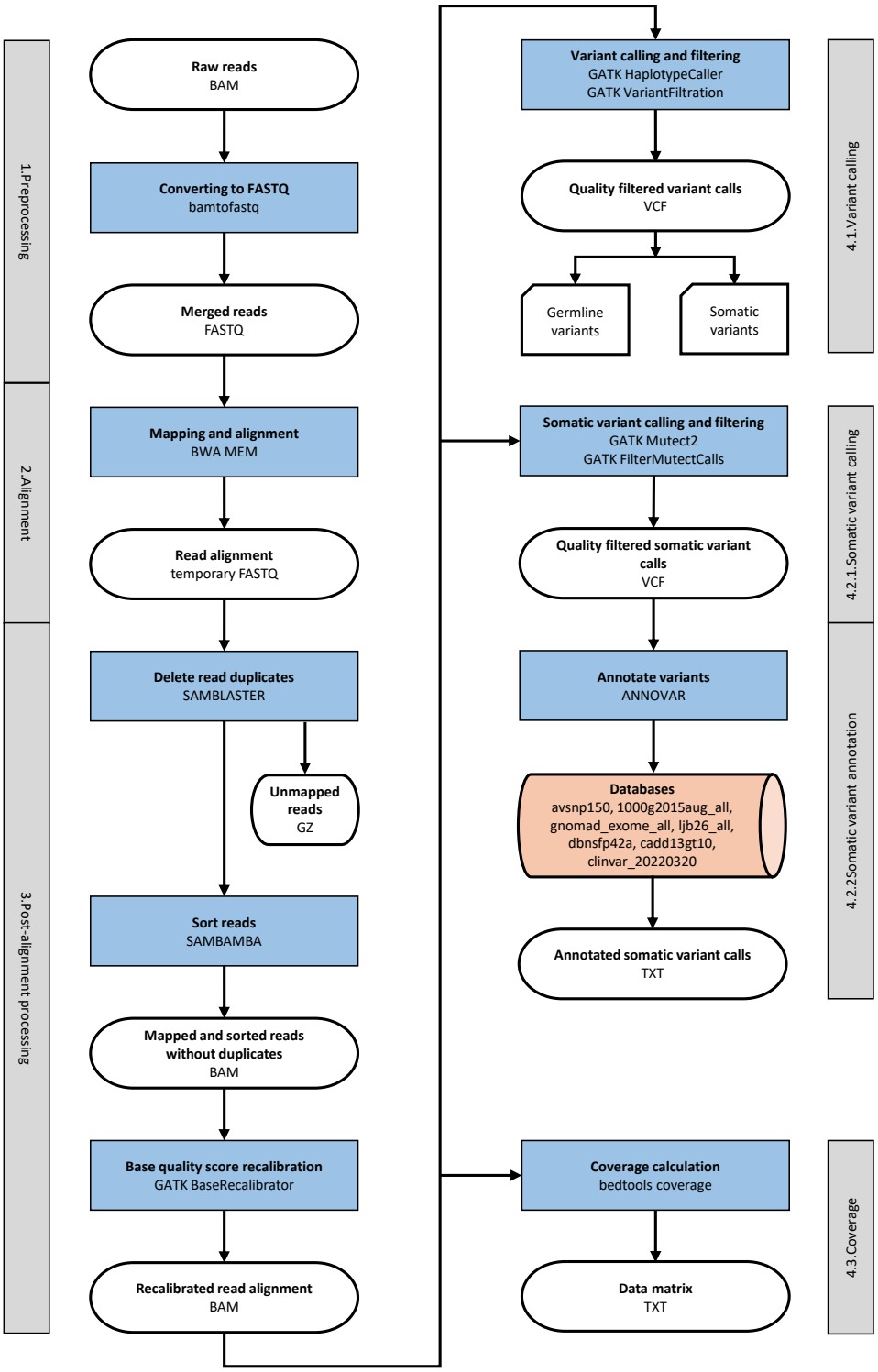

Figure 2.2.: Schematic illustration of processing whole exome sequencing data

2.9. HaplotypeCaller

Principle

HaplotypeCaller can identify single nucleotide polymorphisms (SNPs) and mutations like insertion and deletion. This algorithm finds regions with variations. It rejects the information that exists of the mapping step and rearranges the reads of these regions. The benefits of HaplotypeCaller are that it can call difficult callable areas. It can run with non-diploid organisms or pooled data of an experiment, and it works well with splice junctions which are challenging for other variant callers.

The algorithm uses a database with known variants and a file with analyzed intervals to choose the active regions on which it needs to work. Reassembly of these regions is performed to identify haplotypes, that may exist and are necessary for finding potential variant sites by realigning them to a reference genome. For these variant sites, marginalized allele likelihoods are calculated with pairwise sequencing alignment of each read against every haploid genotype. The allele likelihoods are then used to compute likelihoods of each genotype for every sample and the genotype with the highest score is attached to the sample (GATKTeam, 2023).

Implementation

The previously mapped BAM files were the input for the *HaplotypeCaller* function of the *GATK* package v3.8, which was implemented as .jar file and therefore the *java* package v8 was needed to use this package. As reference genome the FASTA file *human_g1k_v37.fasta*, for the specification of the analyzed intervals the BED file *Twist_Exome_RefSeq_targets_hg19_cleaned.bed*, and as a single nucleotide polymorphism database (dbSNP) of the known variants the VCF file *dbsnp_137.b37.vcf* were used. The non-default settings were: –genotyping_mode DISCOVERY for discovering variants, –min_base_quality_score 5 as treshold for variant calling, -stand_call_conf 10.0 as

treshold for standard calling confidence, –annotateNDA for annotating non-diploid alleles, and -A Coverage, -A MappingQualityZero, -A AlleleBalance, -A DepthPerAlleleBySample and -A FisherStrand for including these in the output.

2.10. Mutect2

Principle

Usage of Mutect2 is calling somatic variants like SNVs, insertions, and deletions by realignment and local assembly. The benefit is that its base relies also on various probability-based models for filtering and assigning genotypes for matched or unmatched samples from the control sample, and for all depths of coverage. This program uses the same reference files as HaplotypeCaller to specify the active regions on which it operates. Identification of possibly existing haplotypes by reassembling these active regions is important for realignment to a reference genome for finding potential variant sites. A likelihood for every read is assigned to every haplotype with pairwise alignment. A matrix with all these likelihoods gets transformed into a matrix with fragment-haplotype likelihoods, and further to a fragment-allele matrix where each haploid genotype varies from the reference genome. These allele likelihoods are used to find the highest genotype score to assign this genotype to the sample.

This outcome is then filtered by another function of GATK called FilterMutectCalls. This function has included many filters. In the first step, it calculates a probability if the found variants are somatic. The next step is to maximize the F-score by choosing a threshold of these probabilities and using this threshold as a hard filter. Other hard filters look at the mapping quality, the supporting bases and if their position is near the end of a read, the amount of variants in local haplotypes, and the length of mismatches between the reference and the variant fragments. Additionally, this function has models based on error probability which calculate several probabilities for example for contamination, for

variants being germline variants, or if a somatic genotype is a representative for a tumor (Benjamin et al., 2019).

Implementation

The input for the *Mutect2* function of the *GATK* package v4.5.0.0 were the BAM files updated with the recalibrated base quality scores. The corresponding *java* package v20 was needed to use this *GATK* package. As reference genome the FASTA file *human_g1k_v37.fasta* and for the specification of the analyzed intervals the BED file *Twist_Exome_RefSeq_targets_hg19_cleaned.bed* were used. The output of *Mutect2* was then filtered by the functions specific filters of *FilterMutectCalls* of the *GATK* package v4.5.0.0

3. Results

3.1. Validation of the presence of the *BRAF V600E* mutation in *in vitro* cell lines

First, we aimed to validate if the *BRAF V600E* mutation is preserved in all our cell lines, which have been established from *BRAF*-mutated tumor tissues. To do so, we performed WES of several models as described in the Materials and Methods section. We used *HaplotypeCaller* and *Mutect2* with *FilterMutectCalls* algorithms to detect mutations by comparing our data to the hg19 human reference genome. The substitution of CAC to CTC on exon 15 of chromosome 7 on position 140,453,136 was detected in all tested models. This substitution is known as the mutation *BRAF V600E* on the complementary strand (Figure 3.1). We next analyzed the variant allelic frequency (VAF) across cell models in the WES data. Our analysis revealed that *BRAF V600E* is detected with 64% VAF in VBT92, the primary treatment-naive subline, with 100% VAF in VBT125, the dabrafenib therapy-refractory recurrence, and with 99% VAF in VBT125Dabra, the *in vitro* dabrafenib-resistant subline (Table 3.1). The increase in VAF of the tumor oncogene *BRAF V600E* in VBT125 versus VBT92 suggests that the patient tumor has evolved into a more aggressive tumor throughout the course of disease. Furthermore, our data show that the propagation of VBT125 into a dabrafenib-resistant subline did not significantly change the *BRAF V600E* VAF.

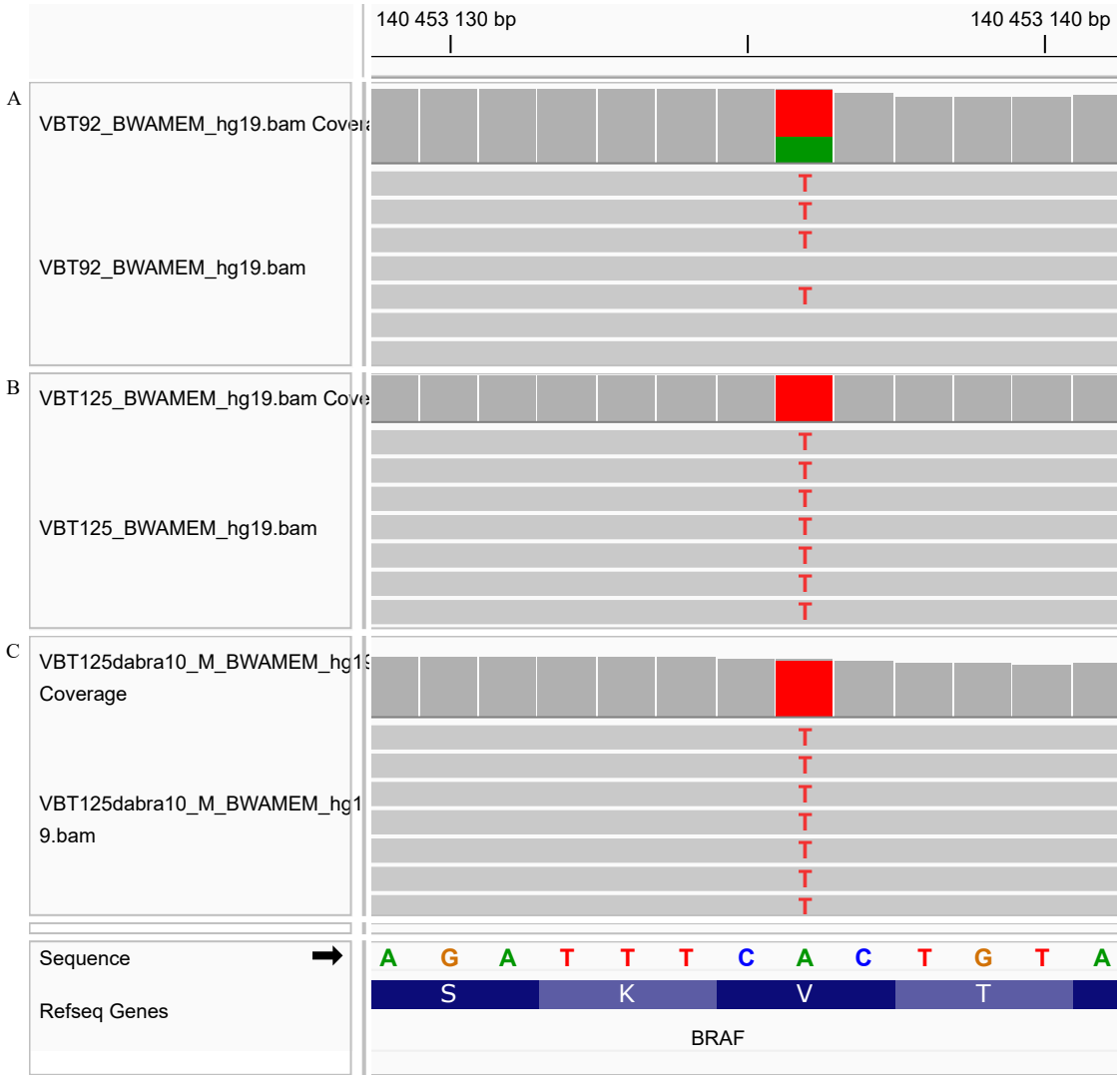

Figure 3.1.: Integrative Genomics Viewer (IGV) output of the WES data, mapped against hg19, showing the substitution of CAC to CTC on exon 15 of chromosome 7 on position 140,453,136, known as *BRAF V600E* mutation, in (A) VBT92, the primary treatment-naive subline, (B) VBT125, the dabrafenib therapy-refractory recurrence and (C) VBT125Dabra the *in vitro* dabrafenib-resistant subline.

As a next step, we validated the *BRAF* gene expression using expression arrays and bulk RNA seq data. We observed that *BRAF* is expressed in all three cell models in expression array as well as in RNA seq data. In line with the presence of the BRAF gain-of-function

mutation, *BRAF* is significantly higher expressed compared to the mean of all other genes in RNA seq data (Table 3.1, Figure 3.2). Surprisingly, this result was not verified in RNA expression arrays where *BRAF* was insignificantly higher expressed compared to all other genes. This is probably due to the fact that *BRAF* was only covered by one probe in the used array format. This suggests that the observed expression levels may be underestimated due to technical limitations, highlighting the importance of validation through alternative methods such as RNA seq.

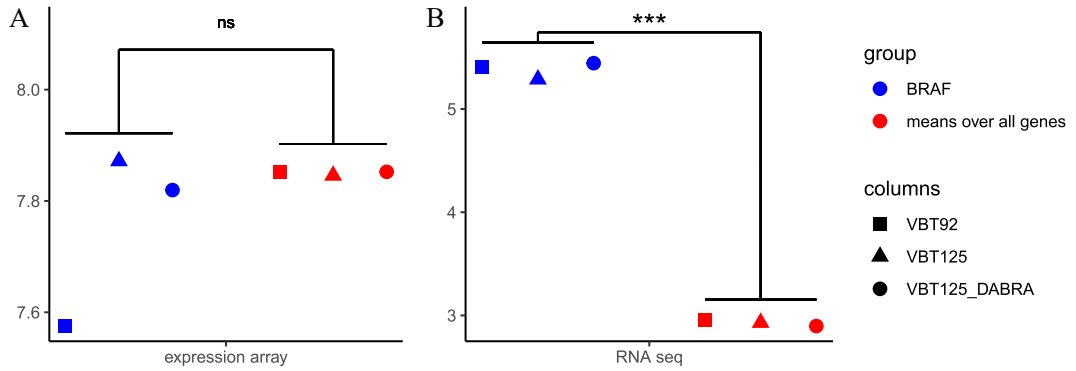

Figure 3.2.: BRAF expression values and the means of expression values of all genes in (A) expression array and (B) RNA seq data of all three cell models with significance calculated by the student's t.test with default parameters: two.sided, paired = FALSE; ns not significant; *** $p < 0.001$.

Table 3.1.: Expression values of BRAF in expression array and RNA seq data, and the VAF dissected from WES data of all three cell lines.

	VBT92	VBT125	VBT125_DABRA
expression arrays	7.58	7.87	7.82
means of arrays	7.85	7.85	7.85
RNA seq	5.41	5.29	5.44
means of RNA seq	2.95	2.93	2.90
VAF (WES)	64% (67/104)	100% (79/79)	99% (80/81)

3.2. Identification of co-mutations in our WES data

We first systematically analyzed the *Mutect2* results of the WES data of VBT125Dabra with VBT125 as reference for previously described genetic co-alterations in *BRAF*-mutated glioma (Schreck et al., 2023). In specific, we explored alterations that were present in VBT125Dabra but not in VBT125 (table 3.2).

Table 3.2.: Co-mutations according to Schreck et al. (2023) found in our WES data of VBT125Dabra but not in VBT125 with location on chromosome, type of alteration, and percentage.

gene	position	alteration	VAF	Mutect2 filter
PDGFRA	chr4: 55,147,766	nonsynonymous SNV	4% (3/68)	weak_evidence
ARID1B	chr6: 157,099,403	nonframeshift deletion	3% (8/260)	haplotype; normal_artifact; slippage
ARID1B	chr6: 157,099,427	nonframeshift deletion	4% (12/278)	haplotype; normal_artifact; slippage
ARID1B	chr6: 157,099,872	nonframeshift deletion	3% (3/113)	normal_artifact; slippage; weak_evidence
ARID1B	chr6: 157,099,982	nonframeshift deletion	2% (3/168)	clustered_events; normal_artifact; slippage; weak_evidence

gene	position	alteration	VAF	Mutect2 filter
ARID1B	chr6: 157,100,117	nonframeshift deletion	1% (3/216)	clustered_events; normal_artifact; slippage; weak_evidence
ARID1B	chr6: 157,100,431	nonframeshift deletion	5% (4/76)	normal_artifact; slippage
MET	chr7: 116,397,784	synonymous SNV	3% (3/101)	weak_evidence
PRKDC	chr8: 48,801,192	unknown	4% C>T (7/197), C>A (3/197)	PASS
PTCH1	chr9: 98,211,390	synonymous SNV	4% (6/151)	PASS
PTEN	chr10: 89,623,861	nonframeshift deletion	94.5% (69/73)	normal_artifact; weak_evidence
CREBBP	chr16: 3,778,303	nonframeshift deletion	2% (5/204)	normal_artifact; slippage
ATRX	chrX: 76,907,782	nonframeshift deletion	2% (3/181)	normal_artifact; slippage; weak_evidence
ARID1B	chr6: 157,100,024	nonframeshift deletion	4% (7/186)	clustered_events; normal_artifact; slippage

Only two co-mutations of our WES data were relevant pathogenic mutations according to *FilterMutectCalls* filtering (filter = PASS). These two mutations are the unknown alteration in *PRKDC* and the synonymous SNV in *PTCH1*.

PRKDC is part of the DNA double-strand break repair and recombination. The alteration was a change from valine (GTC) to isoleucine (ATC) or to phenylalanine (TTC) at chromosome 8 position 48,801,192. Since all three amino acids were nonpolar and hydrophobic, this change is unlikely to cause significant structural alterations in the protein.

PTCH1 is a receptor for the hedgehog signaling pathway and appears to have the function of a tumor suppressor. The synonymous SNV was from isoleucine (ATC) to isoleucine (ATT) on chromosome 9 on position 98,211,390. This leads to the same physicochemical properties (nonpolar/hydrophobic) and is therefore predicted to cause no structural changes in the protein.

PDGFRA and *MET* were labeled with "weak_evidence" which means that there is not enough proof that this is a real mutation. The mutation in *PDGFRA* is a nonsynonymous SNV with a change from glycine (GGC, polar/neutral) to aspartic acid (GAC, acid). Given that *PDGFRA* is downregulated, as observed in chapter 3.3, this mutation may contribute to a loss-of-function. However, further functional studies would be needed to confirm its impact on receptor activity.

The synonymous SNV in *MET* defined a change from asparagine (AAT) to asparagine (AAC), therefore leads to no changes in the protein. MET is a RTK that plays a crucial role in cell signaling. Alterations in *MET* are recognized as oncogenic drivers in human cancer, as overexpression can render receptor activity independent of its ligand, hepatocyte growth factor (HGF). Notably, our RNA seq data (Chapter 3.6) indicate that *HGF* is downregulated, which may further contribute to dysregulated *MET* signaling.

All other mutations were labeled as "normal_artifact" which means that the mutation was also present in the VBT125 thus, was not in relation with resistance development in VBT125Dabra. Together, these data suggest that only the mutation of *PDGFRA* is relevant for dabrafenib-resistance development in this cell model.

Concerning copy number gains and losses, Schreck et al. (2023) highlight losses on

chromosomes 1p and 10, gains on chromosome 7, and gains and losses on 19q in *BRAF*-mutated HGG. Our cell models did not have gains or losses on these chromosomes (see Chapter 3.9). *PDGFRA*, *CDK4/6*, and *KDR* were marked with copy number gains in Schreck et al. (2023), which was not the case in our data. *PTEN* and *CDKN2A/B* were also discovered as genes with CNV losses in *BRAF*-mutated HGG (Schreck et al., 2023), but this was not the case in our data (data not shown).

3.3. Interpretation of up- and downregulated genes and their correlation to pathways

Next, we analyzed top up- and downregulated genes in VBT125Dabra versus VBT125, which was calculated by the expression values of VBT125Dabra minus the expression values of VBT125 using *limma*. Figure 3.3 shows the top and bottom 50 expressed genes of expression arrays and RNA seq ranked by the log fold changes of VBT125Dabra versus VBT125. Comparative analyses of up- and downregulated genes dissected from expression array and RNA seq data revealed significant overlaps, shown in figure 3.4. Shared upregulated genes in expression array and RNA seq data included *IGFBP3*, *CDH4*, and *SAA1*. Shared downregulated genes using both methods included *PDGFRA*, *DUSP6*, *PTPN7*, and *ERG1*.

Using the file of REACTOME pathway collection, containing biological pathways and correlating genes, we next aimed to interpret which pathways and biological functions our top enriched genes are related to. This analysis revealed that *CDH4* and *CLDN1* are involved in the gene sets called *cell-cell communication* and *cell junctions*. *IGFBP3*, belonging to the *transcriptional regulation by TP53* pathway, which is a child term of *RNA Polymerase II transcription* in the REACTOME gene ontology, had the highest logFC value in expression array data (figure 3.3 (A)).

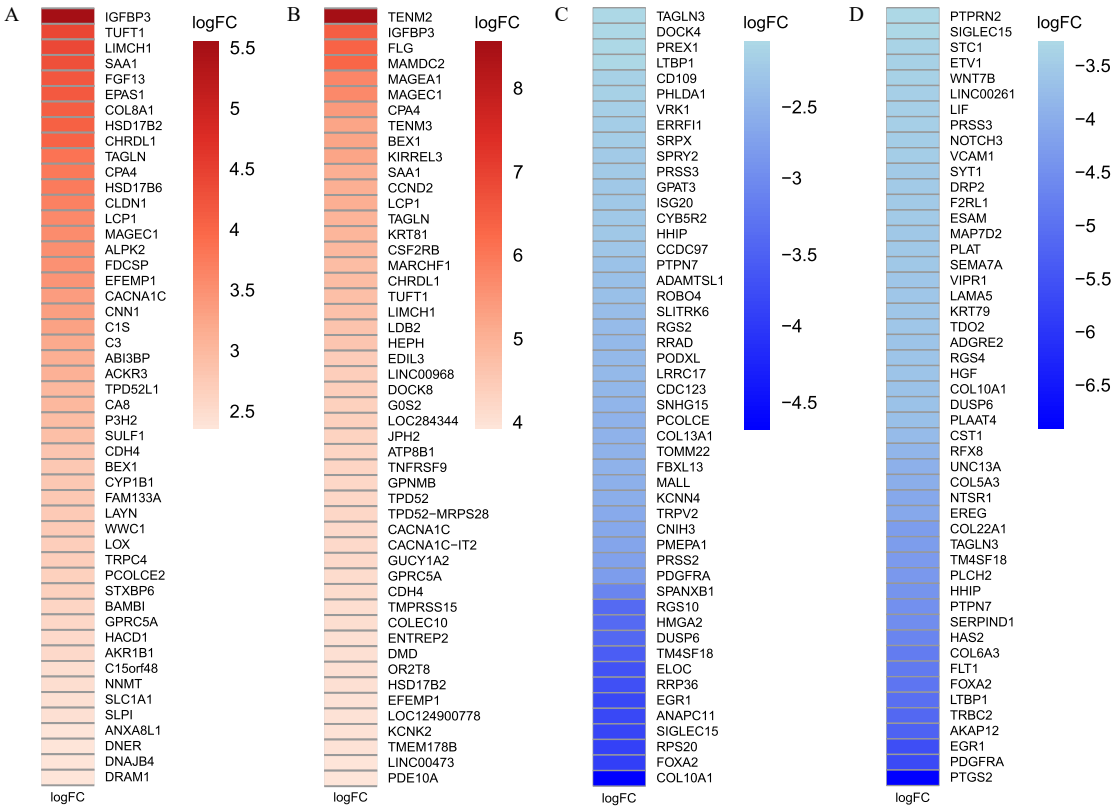

Figure 3.3.: Heatmaps of top and bottom 50 genes ranked by their log fold changes of the contrast VBT125Dabra minus VBT125. Top 50 genes of (A) expression array data and (B) RNA seq data. Bottom 50 genes of (C) expression array data and (D) RNA seq data

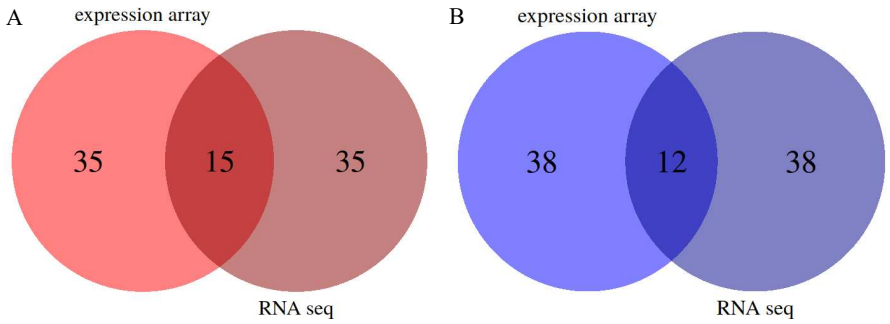

Figure 3.4.: Venn Diagram of top and bottom 50 genes of expression arrays compared to RNA seq. (A) Top 50 genes (B) Bottom 50 genes

Table 3.3.: Expression values of BRAF in expression array and RNA seq data, and the VAF dissected from WES data of all three cell lines.

shared top genes	shared bottom genes
IGFBP3, TUFT1, LIMCH1, SAA1, HSD17B2, CHRDL1, TAGLN, CPA4, LCP1, MAGEC1, EFEMP1, CACNA1C, CDH4, BEX1, GPRC5A	TAGLN3, LTBP1, PRSS3, HHIP, PTPN7, PDGFRA, DUSP6, TM4SF18, EGR1, SIGLEC15, FOXA2, COL10A1

In addition, *ELOC*, a gene of the bottom 50 expression array data, is part of *TP53 regulation of DNA repair genes transcription*. Genes for *negative regulation of the MAPK pathway* (*DUSP6*, *PTPN7*) were among the bottom 50 (figure 3.3 (C)). The tumor suppressor gene *EGR1* is necessary for *PTEN regulation*, which had a lower expression in VBT125Dabra in the expression array data. *DUSP6*, *ERG1*, *PDGFRA*, *RRAD*, and *SPRY2*, which were all downregulated in VBT125Dabra, are important in RTK signaling including the MAPK and the PI3K/AKT pathways. While *DUSP6* is a negative feedback regulator of ERK, *SPRY2* is a negative regulator of RAF in the MAPK pathway.

RNA seq top 50 data (figure 3.3 (B)) also included genes like *CDH4* for *cell-cell communication* and *cell junctions*, and *IGFBP3* for *TP53 regulation of cell death genes transcription* with the second highest logFC value. *CCND2*, which is responsible for *drug-mediated inhibition of CDK4 and CDK6 activity*, was in the RNA seq top 50 data. Bottom 50 data of RNA seq (figure 3.3 (D)) matched many results of bottom 50 expression array data like downregulated *negative regulation of the PI3K/AKT network* pathway (*EREG*, *HGF*, *PDGFRA*), MAPK pathway (*DUSP6*, *EREG*, *HGF*, *PDGFRA*, *PTPN7*), and lower expression of *PTEN regulation* (*EGR1*).

Taken together, in the dabrafenib-resistant VBT125Dabra subline, resistance is likely driven by MAPK pathway reactivation, RTK signaling alterations, PI3K/AKT activation, and cell cycle adaptations. Downregulation of negative regulators (*DUSP6*, *SPRY2*,

PTPN7) suggests loss of MAPK feedback inhibition, while changes in *PDGFRA*, *HGF*, and *EREG* point to RTK reprogramming as a bypass mechanism. Additionally, *ERG1* downregulation may contribute to *PTEN* loss and PI3K/AKT activation, promoting survival despite BRAF inhibition. Upregulation of *CCND2* further indicates *CDK4/6* involvement in resistance. These findings suggest the need for dual- or multi-targeted therapies, such as combining BRAF inhibitors with MEK, RTK, PI3K/AKT, or CDK4/6 inhibitors, to overcome resistance and improve treatment efficacy.

3.4. Exploration of the unsupervised GSEA results

Next, we performed GSEA to investigate up- and downregulated cellular functions in an unsupervised manner. We compared VBT125Dabra versus VBT125 using expression array and RNA seq data. We sorted significant pathways (p.adjust value < 0.05) by their NES value and split them into NES values below (downregulated, Figure A.2 and A.4) and above zero (upregulated, Figure A.1 and A.3). Due to the high number of remaining pathways, we selected pathways that met these inclusion criteria and were in relation to the MAPK pathway or other described crosstalking pathways as shown in figure 3.5. Additionally, pathways that were included in both expression array and RNA seq data were highlighted (Figure 3.5).

Some shared pathways upregulated in VBT125Dabra compared to VBT125 (NES$>$0) included *cell-cell junctions*, *cell adhesion molecules (CAMs)*, and different adhesions between cells in which CAMs are involved. CAMs are important for immune response, inflammation, embryogenesis, hemostasis, and development of neuronal tissue (KEGG Database, 2022). Other upregulated shared pathways relate to actin and myosin filaments in muscle cells and their interactions. These filaments are responsible for muscle contraction such as of the heart which regulates the blood flow and pressure (KEGG Database, 2020). The upregulation of these pathways leads to better survival and better interactions

of the tumor cells resulting in increased invasiveness, and independence of the MAPK pathway (Freemont and Hoyland, 1996; Yamaguchi and Condeelis, 2007).

The three shared pathways downregulated in VBT125Dabra versus VBT125 (NES<0) were *chromosome segregation, interferon alpha/beta signaling, nuclear events kinase and transcription factor activation*, which are important for the cell cycle, the immune system, and the MAPK pathway. This results in poor cell cycle progression, a bypassing of the immune system, and independence of MAPK signaling (Blow and Tanaka, 2005; Tong et al., 2015).

The unsupervised GSEA results of expression arrays (not shared with RNA seq data) with NES higher than zero (Figure 3.5 (A)) included *complement cascade* which leads to better protection of the tumor cells by a survival-promoting microenvironment (Kleczko et al., 2023). *Vascular endothelial growth factor production* pathways were enriched in VBT125Dabra, which leads to formation of abnormal blood vessels, and increased drug efflux which decreases the efficacy of drugs (OGATA et al., 1996; Mou et al., 2024). Upregulation of the *response to toxic substance* pathway means an increase in resistance against toxins and therefore reduction of efficacy (the Gene Ontology, 2025). Higher expression of *regulation of insulin-like growth factor (IGF) transport and uptake by insulin-like growth factor binding proteins (IGFBPs)* and *peptide ligand-binding receptors* pathways could lead to higher expression of IGF which is important for cell proliferation and reactivation of the MAPK pathway (Clément et al., 2018). Upregulation of pathways relating to *cell-cell communication and junction*, as well as *tight junction*, leads to uncontrolled cell proliferation (Garcia et al., 2018). *Organization of vesicles* and formation of *early and late endosomes* are involved in degrading receptors. Upregulation of these pathways can lead to increased recycling or delayed degradation of the receptors which results in activation of the MAPK signaling pathway (Taub et al., 2007). Higher expression of *positive regulation of the MAPK cascade* means upstream reactivation of the MAPK pathway by mutations of RAS or RTKs. The *cell leading edge* is the front part of a cell

involved in cell migration, especially during invasion. This upregulated pathway causes metastasis (Chowdhury et al., 2019).

Additionally, the unsupervised GSEA results of RNA seq (not shared with expression array data) with NES higher than zero (Figure 3.5 (B)) contained *adherens junctions interactions* pathway which belongs to the *cell-cell communication* pathway and therefore to cell proliferation (Garcia et al., 2018). Upregulation of the *negative regulation of T cell receptor signaling* means the pathway is suppressed, and therefore also the anti-tumor response (Laletin et al., 2023).

In the results of the unsupervised GSEA with NES smaller than zero of expression arrays (Figure 3.5 (C)) are several pathways belonging to the cell cycle (*cell cycle checkpoints; cell cycle mitotic - S phase, - M phase - mitotic metaphase and anaphase*). The negative NES of *DNA repair* and *DNA replication* indicated lost DNA repair in VBT125Dabra and might therefore lead to uncontrolled tumor growth (Mercadante and Kasi, 2023). Downregulation of *RNA degradation* and pathways relating to splicing (*spliceosome*, *spliceosomal complex*, *catalytic activity acting on RNA*) could negatively impact efficient gene expression and transcription, leading to higher expression of pro-survival factors (Tian et al., 2015). Lower *signaling by NTRKs* means lower signaling of neurotrophins which are involved in survival and differentiation of neurons via downstream activating the MAPK pathway. This might cause survival independent of the MAPK pathway (Cocco et al., 2019). Reduced telomerase activity (*reference assembly and trafficking of telomerase*) could reduce the replication potential of cells which results in less efficacy of inhibitors (Tomlinson et al., 2006). Downregulation of *neuropeptide receptor activity* can lead to reduced MAPK activation which causes pathway-independent survival and proliferation (Pellieux et al., 2000). *RNA polymerase II transcription termination* pathway with a NES below zero could result in incorrect expression of oncogenes and genes responsible for apoptosis causing resistance to BRAF inhibitors (West and Proudfoot, 2009).

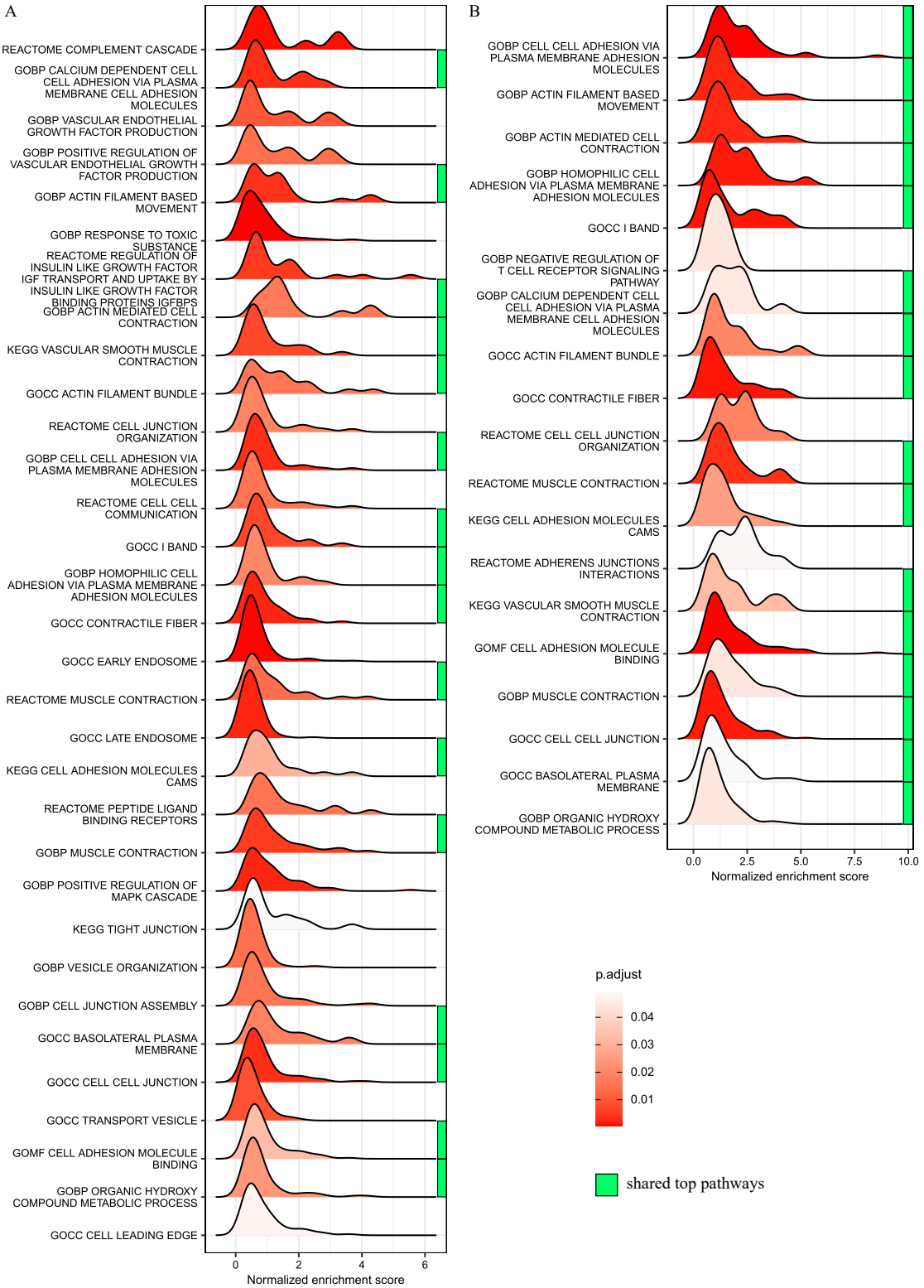
A
REACTOME COMPLEMENT CASCADE
GOBP CALCIUM DEPENDENT CELL CELL ADHESION VIA PLASMA MEMBRANE CELL ADHESION MOLECULES
GOBP VASCULAR ENDOTHELIAL GROWTH FACTOR PRODUCTION
GOBP POSITIVE REGULATION OF VASCULAR ENDOTHELIAL GROWTH FACTOR PRODUCTION
GOBP ACTIN FILAMENT BASED MOVEMENT
GOBP RESPONSE TO TOXIC SUBSTANCE
REACTOME REGULATION OF INSULIN LIKE GROWTH FACTOR IGF TRANSPORT AND UPTAKE BY INSULIN LIKE GROWTH FACTOR BINDING PROTEINS IGFBPS
GOBP ACTIN MEDIATED CELL CONTRACTION
KEGG VASCULAR SMOOTH MUSCLE CONTRACTION
GOCC ACTIN FILAMENT BUNDLE
REACTOME CELL JUNCTION ORGANIZATION
GOBP CELL CELL ADHESION VIA PLASMA MEMBRANE ADHESION MOLECULES
REACTOME CELL CELL COMMUNICATION
GOCC I BAND
GOBP HOMOPHILIC CELL ADHESION VIA PLASMA MEMBRANE ADHESION MOLECULES
GOCC CONTRACTILE FIBER
GOCC EARLY ENDOSOME
REACTOME MUSCLE CONTRACTION
GOCC LATE ENDOSOME
KEGG CELL ADHESION MOLECULES CAMS
REACTOME PEPTIDE LIGAND BINDING RECEPTORS
GOBP MUSCLE CONTRACTION
GOBP POSITIVE REGULATION OF MAPK CASCADE
KEGG TIGHT JUNCTION
GOBP VESICLE ORGANIZATION
GOBP CELL JUNCTION ASSEMBLY
GOCC BASOLATERAL PLASMA MEMBRANE
GOCC CELL CELL JUNCTION
GOCC TRANSPORT VESICLE
GOMF CELL ADHESION MOLECULE BINDING
GOBP ORGANIC HYDROXY COMPOUND METABOLIC PROCESS
GOCC CELL LEADING EDGE
0
2
4
6
Normalized enrichment score
B
GOBP CELL CELL ADHESION VIA PLASMA MEMBRANE ADHESION MOLECULES
GOBP ACTIN FILAMENT BASED MOVEMENT
GOBP ACTIN MEDIATED CELL CONTRACTION
GOBP HOMOPHILIC CELL ADHESION VIA PLASMA MEMBRANE ADHESION MOLECULES
GOCC I BAND
GOBP NEGATIVE REGULATION OF T CELL RECEPTOR SIGNALING PATHWAY
GOBP CALCIUM DEPENDENT CELL CELL ADHESION VIA PLASMA MEMBRANE CELL ADHESION MOLECULES
GOCC ACTIN FILAMENT BUNDLE
GOCC CONTRACTILE FIBER
REACTOME CELL CELL JUNCTION ORGANIZATION
REACTOME MUSCLE CONTRACTION
KEGG CELL ADHESION MOLECULES CAMS
REACTOME ADHERENS JUNCTIONS INTERACTIONS
KEGG VASCULAR SMOOTH MUSCLE CONTRACTION
GOMF CELL ADHESION MOLECULE BINDING
GOBP MUSCLE CONTRACTION
GOCC CELL CELL JUNCTION
GOCC BASOLATERAL PLASMA MEMBRANE
GOBP ORGANIC HYDROXY COMPOUND METABOLIC PROCESS
0.0
2.5
5.0
7.5
10.0
Normalized enrichment score
p.adjust
0.04
0.03
0.02
0.01
shared top pathways

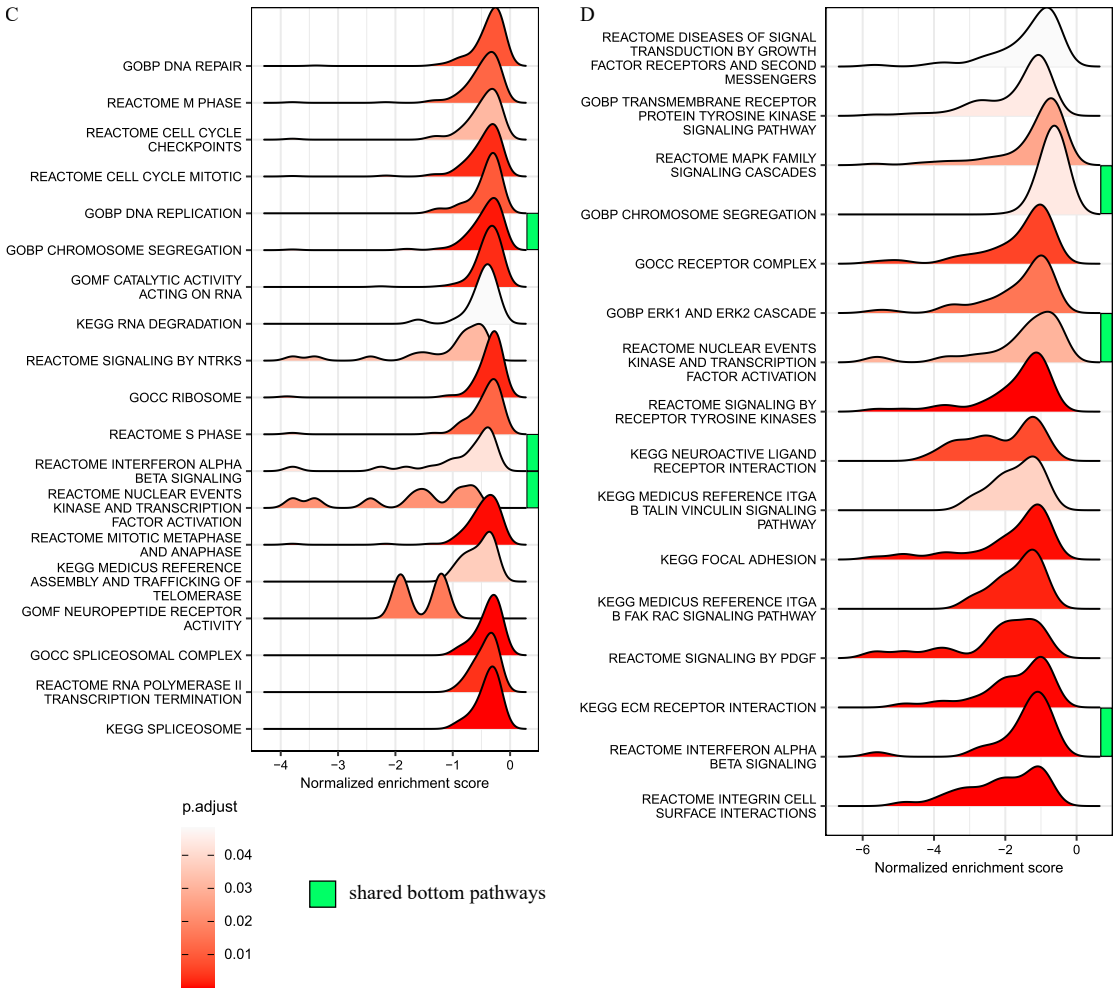

Figure 3.5.: Ridgeline plots of unsupervised GSEA results with VBT125Dabra versus VBT125 filtered by p.adjust < 0.05, split into NES above and below zero and chosen by relevance. Curves were ranked according to their NES. (A) expression array pathways with NES > 0, (B) RNA seq pathways with NES > 0, (C) expression array pathways with NES < 0, (D) RNA seq pathways with NES < 0

The results of the unsupervised GSEA with negative NES of RNA seq (Figure 3.5 (D)) contain *signaling by PDGF*, which is a subpart of *signaling by RTKs*, as well as by *transmembrane receptor protein tyrosine kinases*. These receptors activate amongst others the MAPK pathway. The downregulation of these pathways implicates the downregulation of the *MAPK family signaling cascade* pathway, and therefore also the

negative NES of the *ERK1 and ERK2 cascade*. This means that the VBT125Dabra cells are independent of the MAPK pathway. *Focal adhesion*, *ECM receptor interaction*, and *reference ITGA/B talin vinculin signaling* pathways are important for tumor survival, invasion, and resistance. Therefore, a NES smaller than zero indicates a possible weakening of resistance mechanisms (Li et al., 2021). Reduced *diseases of signal transduction by growth factor receptors and second messengers* (subpathway: oncogenic MAPK signaling), *integrin cell surface interactions*, and *reference ITGA/B FAK RAC signaling* pathways indicate an alternative activation of other survival pathways, therefore independence of MAPK pathway (Lin et al., 1997).

To sum up, some of these pathways show different up- and downregulations that lead to reactivation or less activation of the MAPK signaling pathway. In addition, the results show pathways that cause cell proliferation, invasiveness, poor cell progression, higher drug efflux or inefficacy, and survival without the MAPK pathway in VBT125Dabra compared to VBT125.

3.5. Observation of the GSEA and GSVA results of pathways relating to MAPK pathway

Based on the significant decrease of MAPK pathway genes in the dabrafenib-resistant cell model (*SPRY2*, *DUSP6*, *PDGFRA*, *ERG1*), we suspected independence from the MAPK pathway as one putative resistance mechanism in VBT125Dabra. Therefore, we next analyzed all pathways relating to the MAPK pathway found in the GSEA results, by keyword search using the term "MAPK". We included the pathway collections from REACTOME, KEGG LEGACY and MEDICUS, GOBP, GOCC, and GOMF. The resulting pathways were filtered by the adjusted p-value (<0.2) which shows the probability of false positives in the data. The remaining pathways are shown in ridgeline plots and line plots of these MAPK-related pathways following GSEA and GSVA, respectively (Figure 3.6).

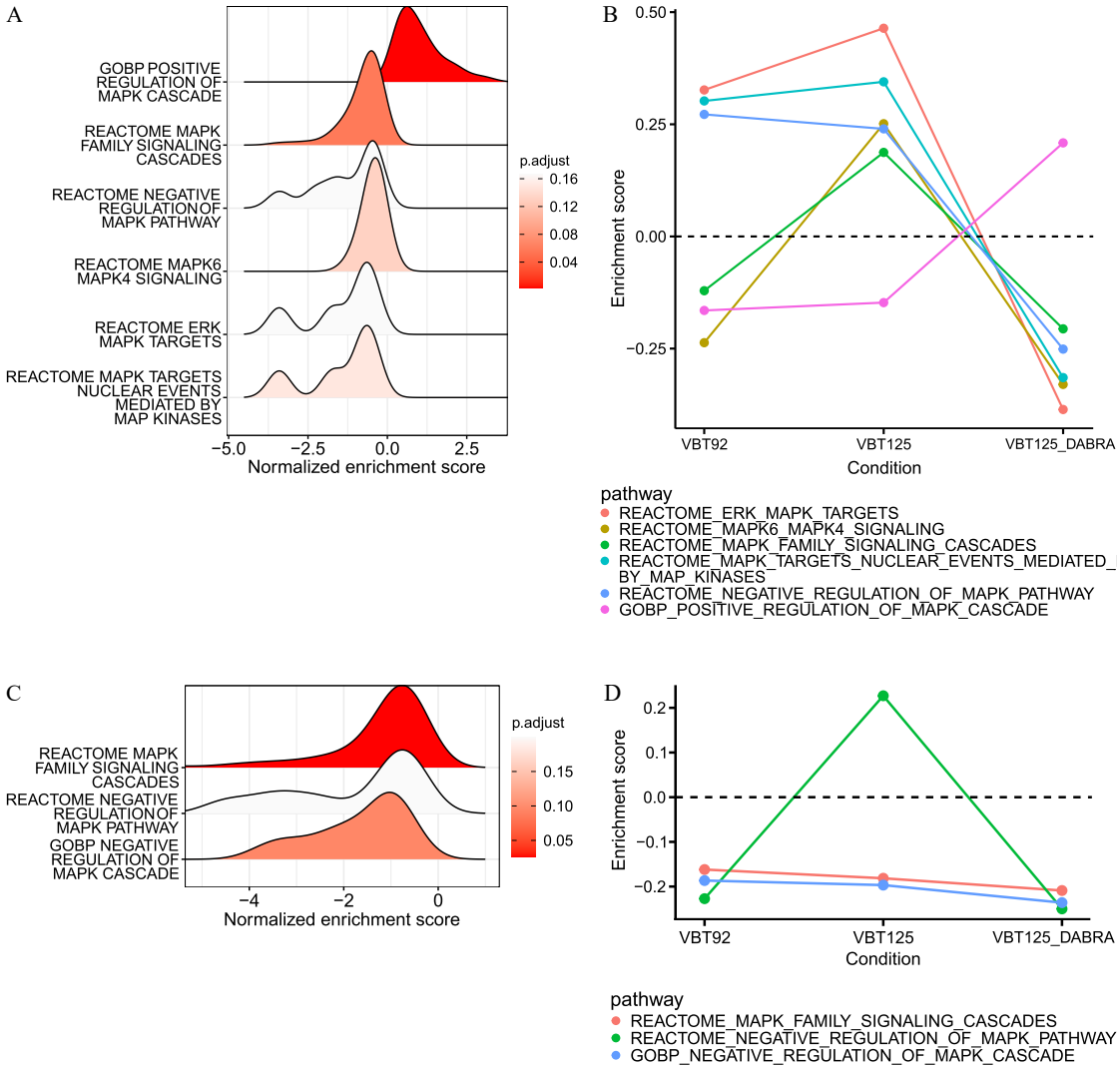

Figure 3.6.: GSEA and GSVA performed with MAPK pathways selected from GMT files of the contrast of VBT125Dabra minus VBT125. The results of GSEA of both sequencing methods filtered by the adjusted p-value of lower than 0.2. These filtered pathways selected from the GSVA data. Ridgeline plot of the NES of the GSEA result of (A) the expression array data and (C) the RNA seq data. Line plot of the ES of the GSVA result of (B) the expression array data and (D) the RNA seq data.

In the GSEA of the expression array data (figure 3.6 (A)), the positive regulation of the MAPK pathway was upregulated in comparison VBT125Dabra versus VBT125 with

a NES of 1.60 and an adjusted p-value of 2.69e-3, and the negative regulation was downregulated with a NES of -1.52 and an adjusted p-value of 1.66e-1. The GSVA output of the expression array data (figure 3.6 (B)) shows that the negative regulation of the MAPK pathway was markedly downregulated and the positive regulation enriched in the resistance cell line VBT125 Dabra in comparison to VBT125. The plot of the RNA seq GSEA data (figure 3.6 (C)) shows that two pathways that were classified for the negative regulation of the MAPK pathway are both downregulated with a NES of -1.53 and -1.60 and adjusted p-values of 1.59e-2 and 2.38e-3. The GSVA data (figure 3.6 (D)) represents the outcome of the GSEA also including the primary cell model VBT92.
Together, these data indicate that the cell lines are independent of the MAPK pathway because important genes involved in this pathway are downregulated.

3.6. Integrative investigation of the genes relating to described resistance mechanisms

Next, we aimed to investigate how our data relate to previously published data. In their review articles,Capogiri et al. (2023) and Lehmann et al. (2022) listed a number of genes that have found to be altered or differentially expressed, which impacts the effect of BRAF inhibitor drugs in cancer cells. We compared our data with the listed genes in these publications. Therefore, we explored their logFC in expression array and RNA seq data, and if they were found with *Mutect2* in VBT125Dabra, but not in VBT125 with parallel analysis of VBT125 as baseline and VBT125Dabra as tumor sample.
Figure 3.7 shows the up- or downregulation of genes, and the resistance mechanism the genes belong to according to Capogiri et al. (2023) and Lehmann et al. (2022) in expression arrays and RNA seq data in the contrast of VBT125 Dabra versus VBT125. Table 3.4 includes mutations found in our WES data of the mentioned genes filtered by *FilterMutectCalls*.

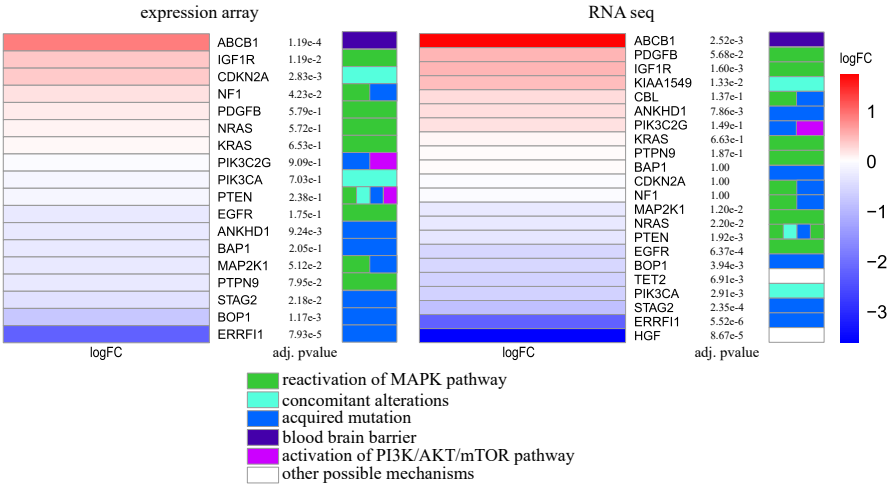

Figure 3.7.: Log fold changes and adjusted p-values of genes of resistance mechanisms in Lehmann et al. (2022) and Capogiri et al. (2023) of the contrast VBT125Dabra minus VBT125 of expression array (left) and RNA seq (right) data. The color code indicates to which resistance mechanism they belong.

The data of both expression arrays and RNA seq showed that *PDGFB* and *IGF1R*, genes involved in reactivation of the MAPK pathway, were significantly upregulated in VBT125Dabra. The upregulation of *PDGFB* is an indicator that it compensates the function of *PDGFRA* which was downregulated (chapter 3.3) and had a nonsynonymous mutation (chapter 3.2), which is thought to cause loss-of-function. *PTPN9*, which is a negative regulator of the VEGFR signaling, was downregulated in VBT125Dabra. *BOP1* was downregulated in both sequencing methods. It is described to acquire mutations upon dabrafenib treatment. Expression of *ABCB1*, known as *P-gp*, is one of the most effective drug efflux pumps, particularly at the BBB, and therefore associated with drug resistance (Capogiri et al., 2023). Expression array and RNA seq data showed significantly higher expression of *ABCB1*, in VBT125Dabra compared to VBT125, suggesting increased drug efflux as one resistance mechanism. *HGF* expression is associated with intrinsic resistance to BRAF inhibitors. LogFC of *HGF* in RNA seq was noticeably negative, so the expression is much lower in VBT125Dabra than in VBT125, which displays that this resistance mechanism is not relevant for our tumor.

3.6. Integrative investigation of the genes relating to described resistance mechanisms

Together, these data again suggest that the observed resistance mechanisms in VBT125Dabra are reactivation of the MAPK pathway with the upregulation of *PDGFB* and *IGF1R*, and higher drug efflux with the upregulation of *ABCB1*.

As a next step, we aimed to explore the resistance genes from Lehmann et al. (2022) and Capogiri et al. (2023) concerning genetic alterations in our WES data.

Table 3.4.: Genes of resistance mechanisms found in WES data with location on chromosome, type of alteration, percentage and filter according to *FilterMutectCalls*; normal_artifact = no new mutation in VBT125Dabra; weak_evidence = not enough reads for proof; slippage = reads with different length than repetitive sequences => technical artifact.

gene	position	alteration	VAF	Mutect2 filter
PTEN	chr10: 89,623,861	nonframeshift deletion	95% (69/73)	normal_artifact; weak_evidence
CBL	chr11: 119,077,233	nonframeshift deletion	2% (4/273)	normal_artifact; slippage; weak_evidence
CBL	chr11: 119,149,356	nonframeshift deletion	2% (4/186)	normal_artifact; slippage

Table 3.4 of such genes contained three deletions according to *Mutect2*. Since *FilterMutectCalls* labeled them as "normal_artifact", these deletions were not important for us. This means that these deletions were also present in VBT125 and are therefore no new mutations in our VBT125Dabra cell line. Together, there are no differential chromosomal alterations in VBT125Dabra in comparison to VBT125 of the genes described in the resistance mechanisms in Lehmann et al. (2022) and Capogiri et al. (2023).

3.7. Identification of other mutations found in our WES results

Further, we observed the remaining mutations in our WES data present in VBt125Dabra but not in VBT125, which are not mentioned in one of the above-named publications. These exonic mutations were filtered by the "PASS" filter and the CADD_raw score between three and four of *FilterMutectCalls* (table 3.5). The PASS filter shows the relevant mutations according to default filters of *FilterMutectCalls* like depth of coverage, base quality, mapping quality, clustered events, duplicate evidence, fragment length, and read position. The CADD_raw (=combined annotation dependent depletion) score between three and four characterizes missense mutations.

Table 3.5.: Further mutations in our WES data present in VBT125Dabra but not in VBT125, with Mutect2 filter = PASS, with location on chromosome, type of alteration, and percentage.

gene	position	alteration	VAF
VWA5B1	chr1: 20,680,535	nonsynonymous SNV	6% (9/144)
RAPGEF2	chr4: 160,277,163	nonsynonymous SNV	5% (12/223)
ISL1	chr5: 50,680,488	nonsynonymous SNV	42% T>C (61/146), T>G (1/146)
UTP15	chr5: 72,866,468	nonsynonymous SNV	55% (62/113)
RXRB	chr6: 33,168,099	nonsynonymous SNV	2% G>A (5/230) + 4 deletions
SLC22A7	chr6: 43,268,874	nonsynonymous SNV	38% T>C (25/66), T>A (2/66)
EPM2A	chr6: 146,056,633	startloss	27% (18/66)
OSGIN2	chr8: 90,926,900	nonsynonymous SNV	5% (10/177)
DMRT3	chr9: 990,869	nonsynonymous SNV	46% (53/114)

gene	position	alteration	VAF
HELLS	chr10: 96,354,583	nonsynonymous SNV	31% (21/68)
DNHD1	chr11: 6,570,011	nonsynonymous SNV	3% (4/149)
HSD17B12	chr11: 43,702,423	nonsynonymous SNV	3% (5/147)
TUBA1C	chr12: 49,666,867	nonsynonymous SNV	42% (103/248)
MLXIP	chr12: 122,622,835	nonsynonymous SNV	36% C>T (39/109), C>A (1/109)
TMEM132C	chr12: 129,180,539	nonsynonymous SNV	7% A>G (11/150), A>T (1/150)
BFAR	chr16: 14,761,514	nonsynonymous SNV	4% (6/153)
KMT2B	chr19: 36,218,099	nonsynonymous SNV	40% (53/133)
CLDN5	chr22: 19,511,235	nonsynonymous SNV	7% (11/163)

Table 3.5 summarizes all detected mutations. The following mutated genes have high priority for our project because alterations of these are linked to MAPK inhibitor resistance: *RAPGEF2* acts upstream in the MAPK pathway, regulates RAP proteins, and a mutation might influence cancer migration and proliferation (Satyanarayana et al., 2010; Shi and Zhang, 2021). *HELLS* is involved in epigenetic regulation which has an impact on genes of the MAPK pathway (Liang et al., 2022). *MLXIP* regulates glycolysis and metabolic processes for oncogenesis support (Fan et al., 2024). *KMT2B* regulates gene expression including genes relating to the MAPK pathway (Zhao et al., 2023).

The following genes have medium priority for our project since the resulting changes in survival, proliferation, and differentiation are indirectly linked to the MAPK pathway: *TUBA1C* is part of the cytoskeletal organization and is known for cancer cell proliferation and motility (Jiang et al., 2023). *OSGIN2* is important for tumor cell survival under treatment (Wang et al., 2023). *RXRB* modulates transcription and cell differentiation (Dawson and Xia, 2012).

The following two genes have lower priority for this master thesis since a link to the MAPK pathway is missing: *SLC22A7* plays a role in drug metabolism which has an impact on the efficacy of MAPK inhibitors, but it has no direct link to MAPK signaling (Ryu et al., 2022). *CLDN5* is involved in cell adhesion and metastasis but only little in MAPK pathways or resistance against inhibitors (Yang et al., 2021).

3.8. Verification of hypersensitivity towards platinum-based compounds

Preliminary large-scale drug screen data from our lab suggested hypersensitivity of VBT125Dabra cells towards platinum-based chemotherapeutics (data not shown). Platinum-based compounds cause DNA damage that interferes with DNA replication and transcription, ultimately triggering cell death (Hu et al., 2016). Therefore, we hypothesized differences in DNA damage response in VBT125Dabra cells. To test this hypothesis, we analyzed differences in pathways of DNA damage, DNA repair, DNA double-strand breakage, and the P53 signaling pathway. "P53", "DNA double-strand break", "DNA damage", "DNA repair", and "DNA replication" were used for key term search to filter selected pathways in the GSEA results (Figure 3.8).

Data from expression arrays and RNA seq aligned very well. Together, data showed a significant upregulation of the TP53 pathway, together with a significant loss of DNA damage response ("SITE OF DNA DAMAGE"), DNA repair, and DNA replication ("GOBP DNA REPLICATION"). These data indeed suggest that VBT125Dabra cells have deficits in repairing platinum compound-induced DNA crosslinks, explaining their observed hypersensitivity towards these chemotherapeutics.

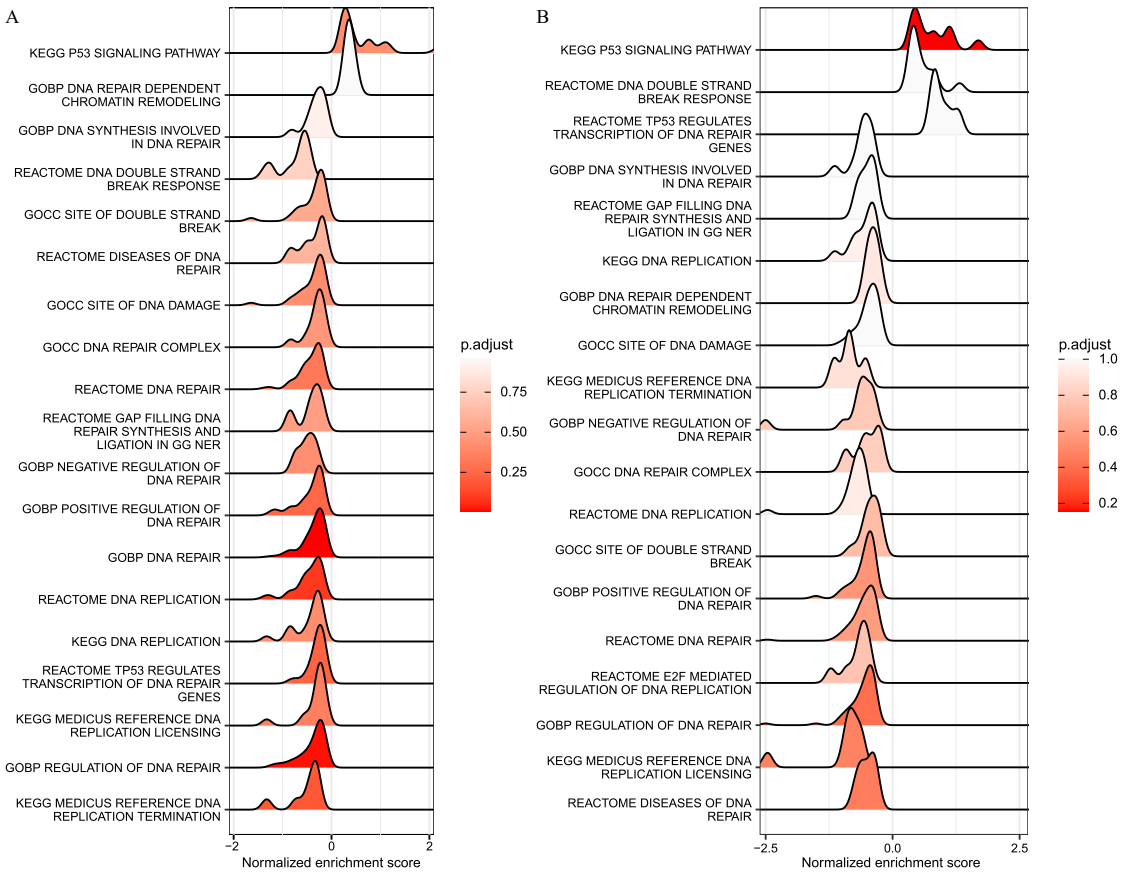

Figure 3.8.: Ridgeline plots of selected pathways of the contrast VBT125Dabra minus VBT125 of (A) expression array and (B) RNA seq GSEA data. The peaks illustrate the normalized enrichment score in the color of the computed adjusted p-value.

3.9. Comparison of copy number variants of WES data

Next, we aimed to compare the whole genome coverage of VBT125Dabra to VBT125 cells. In figure 3.9 the CNVs of the WES data of VBT125 and VBT125Dabra are shown. Orange dots indicate gains (>1.5), blue dots mark losses (<0.6), and gray means normal coverage. Of note, this plot was generated with the means of a total of 40 malignant cell lines across different cancer entities including our three cell models as a reference, since we lacked a non-malignant control sequenced in the same run with our analyses.

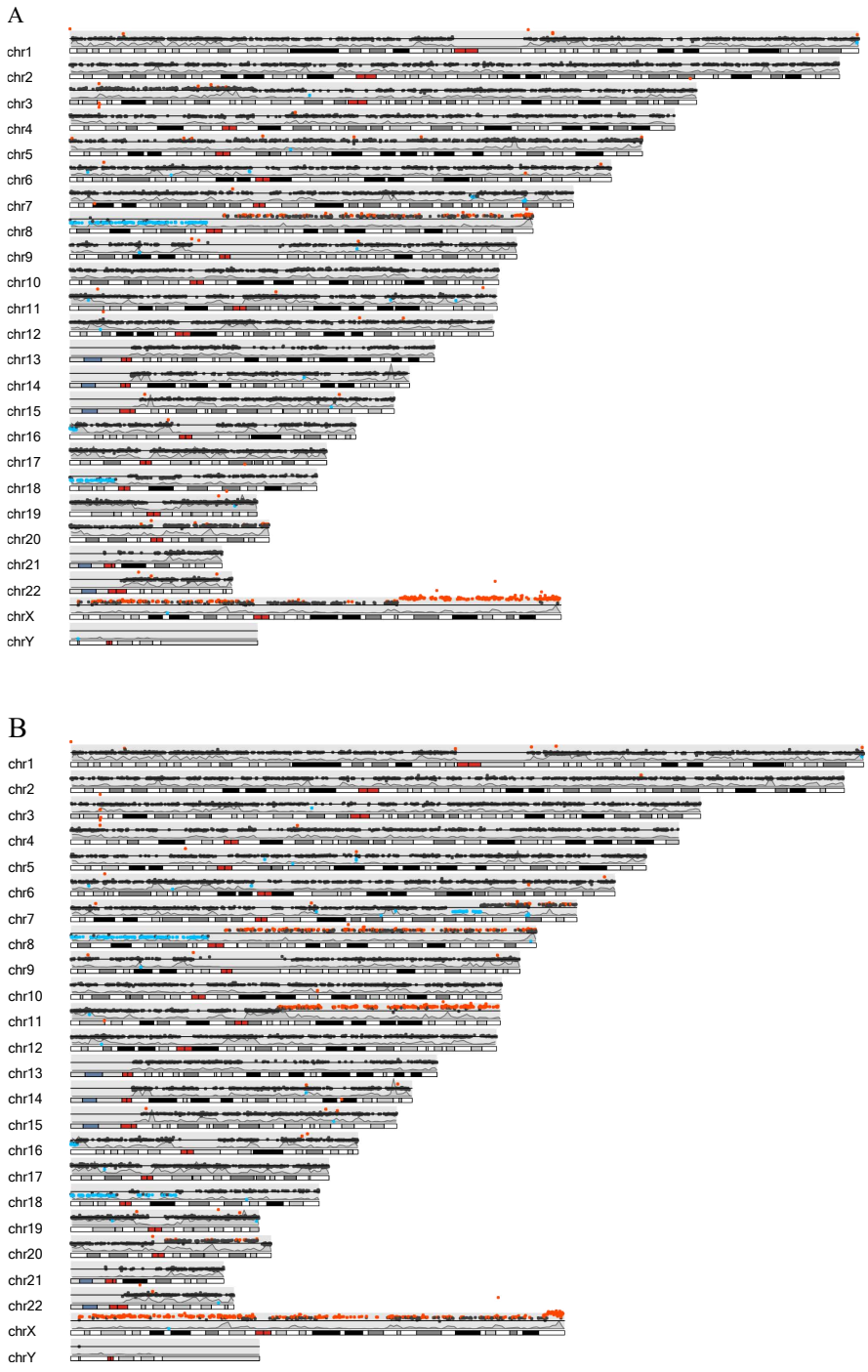

Figure 3.9.: Coverageplots show the CNVs of all chromosomes in the WES data. Orange dots mean the value is above 1.4, which indicates gains, blue means below 0.6, an indication of deletions and gray means normal coverage. A) CNVs of VBT125 B) CNVs of VBT125Dabra

In figure 3.9 (A) the CNVs of VBT125 are shown, indicating losses on chromosome 7p and 18p, and gains on chromosome 8q and all over chromosome X. In figure 3.9 (B) of the CNVs of VBT125Dabra a novel on chromosome 11q gain was observed. This indicates that many genes on chromosome 11q have copy number gains in VBT125Dabra, which are not present in VBT125. Chromosome 11q is a region of interest because many genes belong to DNA replication. This is important for alternative treatment with platinum-based compounds such as cisplatin, oxaliplatin, and carboplatin.

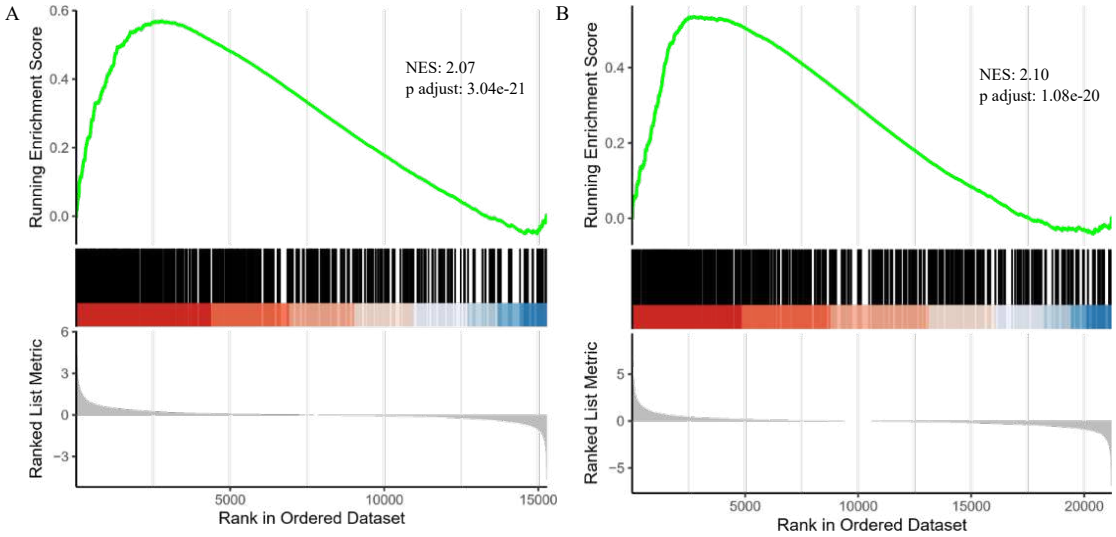

Figure 3.10.: Waterfallplots of the GSEA result with genes on chromosome 11q of the contrast VBT125Dabra minus VBT125 in (A) the expression array data and (B) the RNA seq data.

To prove these results with expression array and RNA seq data, waterfall plots of the GSEA results of chromosome 11q genes were generated (Figure 3.10). To this end, we downloaded a gene set including all genes present on chromosome 11q from `https://ftp.uniprot.org/pub/databases/uniprot/knowledgebase/complete/docs/humchr11.txt` and performed GSEA. In line with the copy number gains on chromosome 11q in the WES data of VBT125Dabra, the GSEA results indicate a significant gene expression enrichment of genes on chromosome 11q using both mRNA expression methods. Based on the

enrichment of genes related to DNA replication and repair on this chromosomal arm, platinum-based compounds, which induce DNA breaks leading to genomic instability and cell death, appear to be a promising alternative treatment for VBT125Dabra cells.

3.10. Investigation of cisplatin resistance

Cisplatin is widely used for different cancer types, but because of intrinsic and acquired resistance, the effectiveness varies between cancer subtypes (Nasimian et al., 2023). To show if our VBT125Dabra cells are sensitive to cisplatin, we chose the genes mentioned in Nasimian et al. (2023) important for cisplatin resistance and looked if the logFC of the expression arrays and RNA seq data matches the results of the paper 3.11.

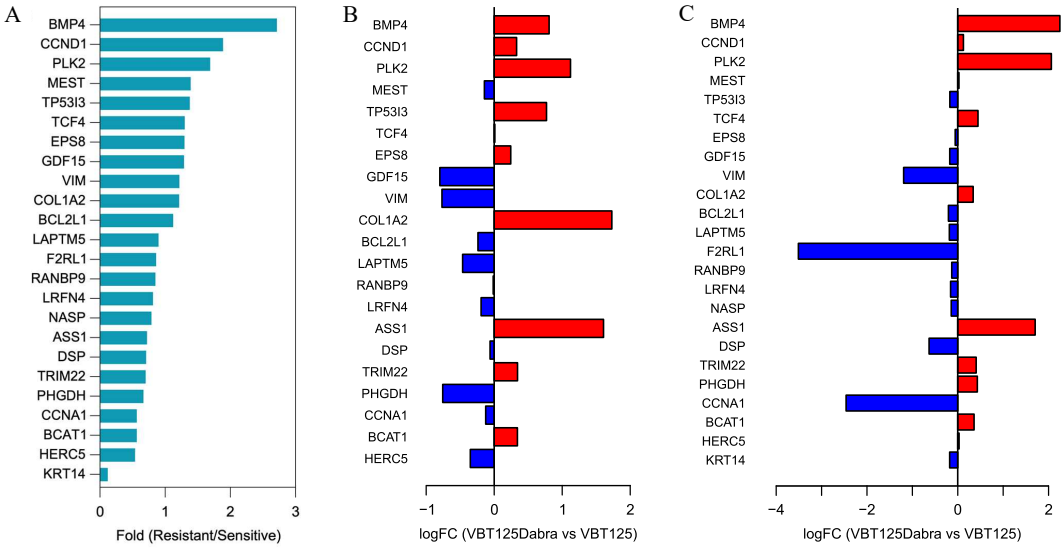

Figure 3.11.: LogFC of resistant versus sensitive cellline of 24 genes important for resistance against cisplatin mentioned in Nasimian et al. (2023). (A) Nasimian et al. (2023) Figure 4B (made available under a Creative Commons license: `https://creativecommons.org/licenses/by/4.0/`), (B) expression array (C) RNA seq

Our data partially aligns with Nasimian et al. (2023), who identified *BCL2L1* as a key factor for cisplatin sensitivity. While we observed a slightly lower expression of *BCL2L1*

in VBT125Dabra, this does not fully confirm cisplatin sensitivity, as other resistance mechanisms could still be active. Further functional validation, including drug response assays and pathway analysis (Chapter 3.8, Chapter 3.9) is needed to assess whether cisplatin and other platinum-based compounds are effective treatment alternatives for VBT125Dabra.

4. Discussion

Pediatric HGGs are aggressive brain tumors associated with poor prognosis and rapid progression depite of multimodal treatment (Ostrom et al., 2022). One of the key molecular drivers in a subset of pediatric HGGs is the *BRAF V600E* mutation, which constitutively activates the MAPK signaling pathway, leading to increased cell survival and uncontrolled tumor growth (Yao et al., 2015). *BRAF V600E* is the most common *BRAF* mutation in several cancer types including melanoma, papillary thyroid carcinoma, and particularly characterizes one subgroup of pediatric HGGs (Capogiri et al., 2023). The identification of this mutation has prompted the development of targeted therapies using BRAF inhibitors like dabrafenib (Davies et al., 2002). These inhibitors have shown significant therapeutic benefits, including improved survival rates and tumor regression in some patients (Long et al., 2014). However, resistance to therapy often develops due to reactivation of the MAPK pathway, secondary mutations, or activation of alternative signaling pathways, limiting long-term efficacy (Capogiri et al., 2023; Lehmann et al., 2022), leaving patients without alternative treatment options.

Therefore, we here aimed at investigating the mechanisms behind acquired resistance to BRAF inhibitors and identifying alternative therapeutics in our in-house generated dabrafenib resistance cell model. A dabrafenib-resistant subline (VBT125Dabra) of one pediatric HGG cell model (VBT125) had been generated in our lab and was compared to its non-resistant counterpart using multi-omics approach involving RNA seq, expression arrays, WES, and a large-scale drug screen in this study.

Underlying resistance mechanism

The most frequently described resistance mechanism against BRAF inhibitors, occurring in around 80% of resistant cases, harboring the *BRAF V600E* mutation is the **reactivation of the MAPK pathway** (Capogiri et al., 2023). This reactivation is frequently due to alternative mutations in the MAPK pathway genes, secondary mutations in BRAF, BRAF copy number gains or fusions, or mutations of RTKs.

Studying the top 50 up- and downregulated genes in VBT125Dabra versus VBT125, we identified several genes of the MAPK pathway like *DUSP6*, *PTPN7*, *PDGFRA*, *ERG1*, and *SPRY2* to be downregulated in VBT125Dabra, indicating that the MAPK pathway is less active in the resistance model compared to VBT125. These results were confirmed by the GSVA and GSEA of several pathways relating to the MAPK pathway, which showed a significant downregulation. Therefore, reactivation of the MAPK pathway can rather be ruled out as resistance mechanism. Instead, our results indicate independence of the MAPK pathway as one possible resistance mechanism. Capogiri et al. (2023) summarized **acquired mutations** in BRAF inhibitor-resistant cancers including *STAG2*, *COT*, *PIK3C2G*, *ERRFI1*, *BAP1*, *ANKHD1*, and *MAP2K1*. None of these mutations was found in our dabrafenib-resistant model (Table 3.4). Screening alternative mutations present in VBT125Dabra but not in VBt125, we only found pathogenic mutations in *PRKDC*, *PTCH1*, and mutations with weak evidence in *PDGFRA*, *MET*, which were synonymous SNVs predicted to cause no structural changes in the protein. The consequences of these mutations remain elusive and must be explored in future studies. The nonsynonymous SNV in *PDGFRA* suggests structural changes in the protein predicting a pathogenic mutation in this gene. Mutations in RTKs have previously been reported in acquired BRAF inhibitor resistance (Du and Lovly, 2018; Lo, 2012, Figure 1). Nevertheless, in expression array and RNA seq data, we observed significant *PDGFRA* downregulation (Figure 3.3), which would rather suggest a loss-of-function mutation. This is contradictory

to the previously reported gain-of-function mutations leading to upregulation of RTKs. Investigation of the logFC data of expression array and RNA seq revealed that two genes (*PDGFB*, *IGF1R*) involved in the reactivation of the MAPK pathway to be upregulated. Upregulation of *PDGFB* could be an adoption of the putative loss-of-function mutation of *PDGFRA*. Wet lab protein expression studies on *PDGFRA* are planned and will help to better understand the functional consequences of the observed mutations on the protein stability and the intracellular location of the receptor.

Concerning gene expression and copy number changes, Capogiri et al. (2023) nominated downregulation of BOP1, loss of *NF1*, *PTEN*, and *CBL*, and activation of *CRAF* to be involved in BRAF inhibitor resistance. *BOP1* was significantly downregulated in expression array and RNA seq data in VBT125Dabra. The mentioned losses and activation were not observed in our data (data not shown). In our WES data, only mutations in PTEN and CBL of the above-mentioned genes were present in VBT125Dabra, but these were also existent in VBT125, and therefore not relevant for resistance development. Further examination of missense mutations in our WES data identified mutations linked to the MAPK signaling pathway with varying degrees of priority. High-priority mutations in *RAPGEF2*, *HELLS*, *MLXIP*, and *KMT2B* directly affect MAPK pathway regulation, while medium-priority mutations in *TUBA1C*, *OSGIN2*, and *RXRB* influence cell differentiation, proliferation, and survival, and low-priority mutations in *SLC22A7* and *CLDN5* impact BRAF inhibitor efficacy and tumor cell interactions. These findings suggest independence of the MAPK pathway by acquired mutations as potential resistance mechanism.

(Capogiri et al., 2023) mentioned **concomitant alterations** like *CDKN2A* deletion, and *BRAF-KIAA1549* fusion, leading to rapid progression of the tumor (Capogiri et al., 2023). However, *CDKN2A* is already lost in the dabrafenib-sensitive model VBT125 (Gabler et al., 2019), and therefore no further investigation was relevant. Secondary mutations in *BRAF* itself or copy number changes in *BRAF* were not detected in VBT125Dabra (data

not shown). No fusion detection tools were used, thus the *BRAF-KIAA1549* fusion could not be confirmed. Therefore, this resistance mechanism does not seem to be relevant for our resistant cell model.

Analyzing the **alternative activation of the PI3K/AKT/mTOR pathway**, induced by activation of *AKT*, mutations in *PIK3C2G*, and loss of *PTEN*, as resistance mechanism (Capogiri et al., 2023; Lehmann et al., 2022; Schreck et al., 2021), revealed no up- or downregulation of these genes in VBT125Dabra. Instead, genes involved in negative regulation of the PI3K/AKT pathway were found in the bottom 50 genes of RNA seq and expression array data suggesting lower expression in VBT125Dabra compared to VBT125. Therefore, activation of the PI3K/AKT/mTOR pathway could indeed be a possible resistance mechanism in our model. This will be studied in detail in Western blot experiments analyzing the protein phosphorylation of PI3K/AKT/mTOR pathway members in the wet lab in future studies.

Importantly, **challenges in drug delivery** or increased efflux of BRAF inhibitors from the cells are observed in resistant cancers (Capogiri et al., 2023). This is frequently due to overexpression of *P-gp* or *BCRP*. Indeed, expression array and RNA seq revealed that *ABCB1* (*P-pg*) is significantly overexpressed in VBT125Dabra, suggesting upregulation of this drug efflux pump.

To sum up, these data suggest that the underlying resistance mechanism in our pediatric HGG line is variable, and likely plays a role at different extents to collectively contribute to dabrafenib resistance. These mechanisms include acquired mutations leading to independence of the MAPK pathway, alternative activation of the PI3K/AKT/mTOR pathway, and increased drug efflux leading to inefficacy of BRAF inhibitors.

Alternative treatment

Combination of surgery, radiotherapy, chemotherapy, and BRAF inhibitors alone or in combination with MEK inhibitors, still leads to the above-mentioned resistance mecha-

nisms (Sasame et al., 2022) in pediatric HGG patients. Therefore, alternative treatment options are essential to improve patient perspectives. Our lab performed a large-scale drug screen (data not shown) which indicates a possible hypersensitivity of VBT125Dabra towards platinum-based compounds like cisplatin, oxaliplatin, and carboplatin. The mode of these chemotherapeutics is the induction of DNA adducts leading to crosslinks and DNA damage (Hu et al., 2016). Consequently, we explored the DNA damage response of our dabrafenib-resistant HGG cells with GSEA. The results of the expression array and RNA seq data indicated a marked upregulation of the TP53 signaling pathway, a significant downregulation of the DNA repair and the DNA damage response pathway, suggesting a deficiency in repairing DNA crosslinks induced by platinum-based compounds (Novakova et al., 2003). CNV analysis of our WES data of VBT125 and VBT125Dabra identified copy number gains of many chromosome 11q genes involved in DNA replication, supporting impaired DNA damage response. Investigation of cisplatin resistance in our VBT125Dabra cells by comparing the logFC results of important resistance genes mentioned in Nasimian et al. (2023), showed only partial agreement with our data. Notably, *BCL2L1*, a key gene implicated in cisplatin resistance (Nasimian et al., 2023), was significantly downregulated in VBT125Dabra in RNA seq, indeed suggesting that our cells are more sensitive to cisplatin.

Together, these results underscore the observed hypersensitivity of our VBT125Dabra cells to platinum-based compounds from our large-scale drug screen, indicating that these chemotherapeutics indeed represent a promising alternative treatment for overcoming BRAF inhibitor resistance in pediatric HGG.

5. Conclusion and Outlook

Summing up, underlying resistance mechanisms for our dabrafenib-resistant pediatric high-grade glioma cell model could be independence of the MAPK pathway via acquired mutations, activation of the PI3K/AKT/mTOR pathway, and increased drug efflux, leading to uncontrolled cell proliferation and survival. A promising alternative treatment option to overcome BRAF-inhibitor resistance seems to be platinum-based chemotherapy due to impaired DNA repair, DNA damage response, and increased TP53 signaling.

Although this thesis involves a multitude of different -omics technologies including expression arrays, RNA seq, and WES, the used data derive from solely one dabrafenib-resistant cell model. This is based on the fact that the generation *in vitro* resistance models from a patient-derived cell model remains challenging and, consequently, is rare. To compensate this putative drawback, we integrated several publicly available data and landscape studies into this thesis. Still, this project included among first analyses of resistance mechanisms and alternative treatment options in patient-derived pediatric HGG cell models, and therefore, further investigations for a more precise insight are necessary. Accordingly, a second cell line was made dabrafenib-resistant *in vitro* to analyze if the results remain the same as shown in this thesis. The workflows and scripts I developed for processing and analyzing of the expression array, RNA seq, and WES data will be significant for further analyses. Furthermore, a bachelor's student conducted a parallel wet lab-focused study alongside this master's thesis. The wet lab data are well in alignment with the *in silico* findings of this thesis and are currently being connected for scientific publication.

Together, this master thesis improves the understanding of resistance mechanisms of pediatric HGGs and suggets a possible alternative therapy.

List of Tables

List of Figures

6. Abbreviations

BRAF V-raf murine viral oncogene homolog B1

BP biological process

BBB blood-brain barrier

CADD combined annotation dependent depletion

CC cellular component

cDNA complementary DNA

CNS central nervous system

CNVs copy number variations

cRNA complementary RNA

DGEList Digital Gene Expression data list

DIPG diffuse intrinsic pontine gliomas

ERK extracellular-signal-regulated kinases

ES enrichment score

FDA US Food and Drug Administration

GATK Genome Analysis Toolkit

gDNA genomic DNA

GMT Gene Matrix Transposed files

GSEA gene set enrichment analysis

GSVA gene set variation analysis

HGF hepatocyte growth factor

HGGs high-grade gliomas

IC50 half-maximal inhibitory concentration

IDH isocitrate dehydrogenase

logFC $\log_2$ fold changes

MAPK mitogen-activated protein kinase

MEK mitogen-activated protein kinase kinase

MF molecular function

MSigDB Molecular Signature Database

NES normalized enrichment score

NGS Next Generation Sequencing

OS overall survival

PMC PubMed Central

RAF rapidly accelerated fibrosarcoma

RAS rat sarcoma protein

RNA seq RNA sequencing

RTKs receptor tyrosine kinases

SNPs single nucleotide polymorphisms

SNVs single number variations

TMZ temozolomide

VAF variant allelic frequency

VBT Vienna Brain Tumor

WES whole exome sequencing

WHO World Health Organisation

Bibliography

American Childhood Cancer Organization (2018). Causes, risk factors, and prevention of childhood brain tumor cancer. https://www.acco.org/blog/causes-risk-factors-and-prevention-of-childhood-brain-tumor-cancer/ [Accessed: July 2024].

Bartha, Á. and Győrffy, B. (2019). Comprehensive outline of whole exome sequencing data analysis tools available in clinical oncology. *Cancers*, 11(11):1725.

Benjamin, D., Sato, T., Cibulskis, K., Getz, G., Stewart, C., and Lichtenstein, L. (2019). Calling somatic snvs and indels with mutect2. *BioRxiv*, page 861054.

Blow, J. J. and Tanaka, T. U. (2005). The chromosome cycle: coordinating replication and segregation: second in the cycles review series. *EMBO reports*, 6(11):1028–1034.

Brock, C. S., Newlands, E. S., Wedge, S. R., Bower, M., Evans, H., Colquhoun, I., Roddie, M., Glaser, M., Brampton, M. H., and Rustin, G. J. (1998). Phase i trial of temozolomide using an extended continuous oral schedule. *Cancer research*, 58(19):4363–4367.

Capogiri, M., De Micheli, A. J., Lassaletta, A., Muñoz, D. P., Coppé, J.-P., Mueller, S., and Guerreiro Stucklin, A. S. (2023). Response and resistance to brafv600e inhibition in gliomas: Roadblocks ahead? *Frontiers in Oncology*, 12:1074726.

Castel, D., Philippe, C., Calmon, R., Le Dret, L., Truffaux, N., Boddaert, N., Pagès, M., Taylor, K. R., Saulnier, P., Lacroix, L., et al. (2015). Histone h3f3a and hist1h3b

k27m mutations define two subgroups of diffuse intrinsic pontine gliomas with different prognosis and phenotypes. *Acta neuropathologica*, 130:815–827.

Chaichana, K. L., Jusue-Torres, I., Navarro-Ramirez, R., Raza, S. M., Pascual-Gallego, M., Ibrahim, A., Hernandez-Hermann, M., Gomez, L., Ye, X., Weingart, J. D., et al. (2014). Establishing percent resection and residual volume thresholds affecting survival and recurrence for patients with newly diagnosed intracranial glioblastoma. *Neuro-oncology*, 16(1):113–122.

Chowdhury, F. N., Reisinger, J., Gomez, K. E., Chimed, T.-S., Thomas, C. M., Le, P. N., Miller, B., Morton, J. J., Nieto, C. M., Somerset, H. L., et al. (2019). Leading edge or tumor core: Intratumor cancer stem cell niches in oral cavity squamous cell carcinoma and their association with stem cell function. *Oral oncology*, 98:118–124.

Clément, F., Martin, A., Venara, M., de Luján Calcagno, M., Mathó, C., Maglio, S., Lombardi, M. G., Bergadá, I., and Pennisi, P. A. (2018). Type 1 igf receptor localization in paediatric gliomas: significant association with who grading and clinical outcome. *Hormones and Cancer*, 9:205–214.

Cocco, E., Schram, A. M., Kulick, A., Misale, S., Won, H. H., Yaeger, R., Razavi, P., Ptashkin, R., Hechtman, J. F., Toska, E., et al. (2019). Resistance to trk inhibition mediated by convergent mapk pathway activation. *Nature medicine*, 25(9):1422–1427.

Davies, H., Bignell, G. R., Cox, C., Stephens, P., Edkins, S., Clegg, S., Teague, J., Woffendin, H., Garnett, M. J., Bottomley, W., et al. (2002). Mutations of the braf gene in human cancer. *Nature*, 417(6892):949–954.

Dawson, M. I. and Xia, Z. (2012). The retinoid x receptors and their ligands. *Biochimica et Biophysica Acta (BBA)-Molecular and Cell Biology of Lipids*, 1821(1):21–56.

Du, Z. and Lovly, C. M. (2018). Mechanisms of receptor tyrosine kinase activation in cancer. *Molecular cancer*, 17:1–13.

Fan, Y., Ge, Y., Niu, K., Li, Y., Qi, L.-W., Zhu, H., and Ma, G. (2024). Mlxipl associated with tumor-infiltrating cd8+ t cells is involved in poor prostate cancer prognosis. *Frontiers in Immunology*, 15:1364329.

Freemont, A. and Hoyland, J. (1996). Cell adhesion molecules. *Clinical molecular pathology*, 49(6):M321.

Gabler, L., Lötsch, D., Kirchhofer, D., van Schoonhoven, S., Schmidt, H. M., Mayr, L., Pirker, C., Neumayer, K., Dinhof, C., Kastler, L., et al. (2019). Tert expression is susceptible to braf and ets-factor inhibition in braf v600e/tert promoter double-mutated glioma. *Acta neuropathologica communications*, 7:1–16.

Garcia, M. A., Nelson, W. J., and Chavez, N. (2018). Cell–cell junctions organize structural and signaling networks. *Cold Spring Harbor perspectives in biology*, 10(4):a029181.

GATKTeam (2023). Haplotypecaller – gatk. `https://gatk.broadinstitute.org/hc/en-us/articles/360037225632-HaplotypeCaller` [Accessed: May 2024].

Guidi, M., Giunti, L., Buccoliero, A. M., Caporalini, C., Censullo, M. L., Galli, L., Genitori, L., and Sardi, I. (2021). Genetic signature and treatment of pediatric high-grade glioma. *Molecular and Clinical Oncology*, 14(4):1–1.

Hall-Jackson, C. A., Eyers, P. A., Cohen, P., Goedert, M., Boyle, F. T., Hewitt, N., Plant, H., and Hedge, P. (1999). Paradoxical activation of raf by a novel raf inhibitor. *Chemistry & biology*, 6(8):559–568.

Hänzelmann, S., Castelo, R., and Guinney, J. (2013). Gsva: gene set variation analysis for microarray and rna-seq data. *BMC bioinformatics*, 14:1–15.

Hingorani, M., Colley, W. P., Dixit, S., and Beavis, A. M. (2012). Hypofractionated radiotherapy for glioblastoma: strategy for poor-risk patients or hope for the future? *The British journal of radiology*, 85(1017):e770–e781.

Hu, J., Lieb, J. D., Sancar, A., and Adar, S. (2016). Cisplatin dna damage and repair maps of the human genome at single-nucleotide resolution. *Proceedings of the National Academy of Sciences*, 113(41):11507–11512.

Jiang, Y., Zhu, C., Huang, H., Huang, G., Fu, B., and Xi, X. (2023). Tuba1c is a potential new prognostic biomarker and promotes bladder urothelial carcinoma progression by regulating the cell cycle. *BMC cancer*, 23(1):716.

Jones, C., Karajannis, M. A., Jones, D. T., Kieran, M. W., Monje, M., Baker, S. J., Becher, O. J., Cho, Y.-J., Gupta, N., Hawkins, C., et al. (2017). Pediatric high-grade glioma: biologically and clinically in need of new thinking. *Neuro-oncology*, 19(2):153–161.

Joseph, E. W., Pratilas, C. A., Poulikakos, P. I., Tadi, M., Wang, W., Taylor, B. S., Halilovic, E., Persaud, Y., Xing, F., Viale, A., et al. (2010). The raf inhibitor plx4032 inhibits erk signaling and tumor cell proliferation in a v600e braf-selective manner. *Proceedings of the National Academy of Sciences*, 107(33):14903–14908.

Karajannis, M. A., Legault, G., Fisher, M. J., Milla, S. S., Cohen, K. J., Wisoff, J. H., Harter, D. H., Goldberg, J. D., Hochman, T., Merkelson, A., et al. (2014). Phase ii study of sorafenib in children with recurrent or progressive low-grade astrocytomas. *Neuro-oncology*, 16(10):1408–1416.

KEGG Database (2020). Kegg pathway: Map04270. https://www.kegg.jp/entry/map04270 [Accessed: February 2025].

KEGG Database (2022). Kegg pathway: Map04514. https://www.kegg.jp/entry/map04514 [Accessed: February 2025].

Khuong-Quang, D.-A., Buczkowicz, P., Rakopoulos, P., Liu, X.-Y., Fontebasso, A. M., Bouffet, E., Bartels, U., Albrecht, S., Schwartzentruber, J., Letourneau, L., et al. (2012). K27m mutation in histone h3. 3 defines clinically and biologically distinct subgroups of pediatric diffuse intrinsic pontine gliomas. *Acta neuropathologica*, 124:439–447.

Kleczko, E. K., Poczobutt, J. M., Navarro, A. C., Laskowski, J., Johnson, A. M., Korpela, S. P., Gurule, N. J., Heasley, L. E., Hopp, K., Weiser-Evans, M. C., et al. (2023). Upregulation of complement proteins in lung cancer cells mediates tumor progression. *Frontiers in Oncology*, 12:1045690.

Knapen, D., Vergauwen, L., Laukens, K., and Blust, R. (2009). Best practices for hybridization design in two-colour microarray analysis. *Trends in biotechnology*, 27(7):406–414.

Koumaki, K., Kontogianni, G., Kosmidou, V., Pahitsa, F., Kritsi, E., Zervou, M., Chatzioannou, A., Souliotis, V. L., Papadodima, O., and Pintzas, A. (2021). Braf paradox breakers plx8394, plx7904 are more effective against brafv600e crc cells compared with the braf inhibitor plx4720 and shown by detailed pathway analysis. *Biochimica et Biophysica Acta (BBA)-Molecular Basis of Disease*, 1867(4):166061.

Kowalewski, A., Durślewicz, J., Zdrenka, M., Grzanka, D., and Szylberg, Ł. (2020). Clinical relevance of braf v600e mutation status in brain tumors with a focus on a novel management algorithm. *Targeted Oncology*, 15:531–540.

Kukurba, K. R. and Montgomery, S. B. (2015). Rna sequencing and analysis. *Cold Spring Harbor Protocols*, 2015(11):pdb–top084970.

Laletin, V., Bernard, P.-L., da Silva, C. C., Guittard, G., and Nunes, J. A. (2023). Negative intracellular regulators of t-cell receptor (tcr) signaling as potential antitumor immunotherapy targets. *Journal for Immunotherapy of Cancer*, 11(5).

Lehmann, R., Rayner, B., and Ziegler, D. (2022). Resistance mechanisms in brafv600e paediatric high-grade glioma and current therapeutic approaches. *Frontiers in oncology*, 12:1031378.

Li, H., Wang, G., Wang, W., Pan, J., Zhou, H., Han, X., Su, L., Ma, Z., Hou, L., and Xue, X. (2021). A focal adhesion-related gene signature predicts prognosis in glioma

and correlates with radiation response and immune microenvironment. *Frontiers in Oncology*, 11:698278.

Liang, X., Li, L., and Fan, Y. (2022). Diagnostic, prognostic, and immunological roles of hells in pan-cancer: A bioinformatics analysis. *Frontiers in Immunology*, 13:870726.

Lin, T. H., Aplin, A. E., Shen, Y., Chen, Q., Schaller, M., Romer, L., Aukhil, I., and Juliano, R. (1997). Integrin-mediated activation of map kinase is independent of fak: evidence for dual integrin signaling pathways in fibroblasts. *The Journal of cell biology*, 136(6):1385–1395.

Lo, R. S. (2012). Receptor tyrosine kinases in cancer escape from braf inhibitors. *Cell research*, 22(6):945–947.

Long, G. V., Stroyakovskiy, D., Gogas, H., Levchenko, E., de Braud, F., Larkin, J., Garbe, C., Jouary, T., Hauschild, A., Grob, J. J., et al. (2014). Combined braf and mek inhibition versus braf inhibition alone in melanoma. *New England Journal of Medicine*, 371(20):1877–1888.

Louis, D. N., Perry, A., Wesseling, P., Brat, D. J., Cree, I. A., Figarella-Branger, D., Hawkins, C., Ng, H., Pfister, S. M., Reifenberger, G., et al. (2021). The 2021 who classification of tumors of the central nervous system: a summary. *Neuro-oncology*, 23(8):1231–1251.

Mackenzie, R. J. (2018). Rna-seq: Basics, applications and protocol. *Technol. Netw. Genom. Res.*

Mercadante, A. A. and Kasi, A. (2023). Genetics, cancer cell cycle phases. In *StatPearls [Internet]*. StatPearls Publishing.

Mittapalli, R. K., Vaidhyanathan, S., Dudek, A. Z., and Elmquist, W. F. (2013). Mechanisms limiting distribution of the threonine-protein kinase b-rafv600e inhibitor

dabrafenib to the brain: implications for the treatment of melanoma brain metastases. *Journal of Pharmacology and Experimental Therapeutics*, 344(3):655–664.

Mou, J., Li, C., Zheng, Q., Meng, X., and Tang, H. (2024). Research progress in tumor angiogenesis and drug resistance in breast cancer. *Cancer Biology & Medicine*, 21(7):571.

Nasimian, A., Ahmed, M., Hedenfalk, I., and Kazi, J. U. (2023). A deep tabular data learning model predicting cisplatin sensitivity identifies bcl2l1 dependency in cancer. *Computational and Structural Biotechnology Journal*, 21:956–964.

National Cancer Institute (2024). glioma. https://www.cancer.gov/publications/dictionaries/cancer-terms/def/glioma [Accessed: July 2024].

NHS inform (2024). Malignant brain tumour (cancerous). https://www.nhsinform.scot/illnesses-and-conditions/cancer/cancer-types-in-adults/malignant-brain-tumour-cancerous/ [Accessed: July 2024].

Novakova, O., Kasparkova, J., Malina, J., Natile, G., and Brabec, V. (2003). Dna–protein cross-linking by trans-[ptcl 2 (e-iminoether) 2]. a concept for activation of the trans geometry in platinum antitumor complexes. *Nucleic acids research*, 31(22):6450–6460.

Oberholzer, P. A., Kee, D., Dziunycz, P., Sucker, A., Kamsukom, N., Jones, R., Roden, C., Chalk, C. J., Ardlie, K., Palescandolo, E., et al. (2012). Ras mutations are associated with the development of cutaneous squamous cell tumors in patients treated with raf inhibitors. *Journal of clinical oncology*, 30(3):316–321.

OGATA, Y., HARADA, Y., FUJII, T., YAMANA, H., FUJITA, H., and SHIROUZU, K. (1996). Immunohistochemical localization of vascular endothelial growth factor in esophageal cancer. *The Kurume Medical Journal*, 43(2):157–163.

Ostrom, Q. T., De Blank, P. M., Kruchko, C., Petersen, C. M., Liao, P., Finlay, J. L., Stearns, D. S., Wolff, J. E., Wolinsky, Y., Letterio, J. J., et al. (2015). Alex's lemonade

stand foundation infant and childhood primary brain and central nervous system tumors diagnosed in the united states in 2007–2011. *Neuro-oncology*, 16(suppl_10):x1–x36.

Ostrom, Q. T., Price, M., Ryan, K., Edelson, J., Neff, C., Cioffi, G., Waite, K. A., Kruchko, C., and Barnholtz-Sloan, J. S. (2022). Cbtrus statistical report: pediatric brain tumor foundation childhood and adolescent primary brain and other central nervous system tumors diagnosed in the united states in 2014–2018. *Neuro-oncology*, 24(Supplement_3):iii1–iii38.

PDQ Pediatric Treatment Editorial Board (2019). Childhood brain and spinal cord tumors treatment overview (pdq ®). In *PDQ Cancer Information Summaries [Internet]*. National Cancer Institute (US).

Pellieux, C., Sauthier, T., Domenighetti, A., Marsh, D. J., Palmiter, R. D., Brunner, H.-R., and Pedrazzini, T. (2000). Neuropeptide y (npy) potentiates phenylephrine-induced mitogen-activated protein kinase activation in primary cardiomyocytes via npy y5 receptors. *Proceedings of the National Academy of Sciences*, 97(4):1595–1600.

Polier, S., Samant, R. S., Clarke, P. A., Workman, P., Prodromou, C., and Pearl, L. H. (2013). Atp-competitive inhibitors block protein kinase recruitment to the hsp90-cdc37 system. *Nature chemical biology*, 9(5):307–312.

Pollack, I. F., Agnihotri, S., and Broniscer, A. (2019). Childhood brain tumors: current management, biological insights, and future directions: Jnspg 75th anniversary invited review article. *Journal of Neurosurgery: Pediatrics*, 23(3):261 – 273.

Price, M., Ballard, C., Benedetti, J., Neff, C., Cioffi, G., Waite, K. A., Kruchko, C., Barnholtz-Sloan, J. S., and Ostrom, Q. T. (2024). Cbtrus statistical report: primary brain and other central nervous system tumors diagnosed in the united states in 2017–2021. *Neuro-oncology*, 26(Supplement_6):vi1–vi85.

Reiner, A., Yekutieli, D., and Benjamini, Y. (2003). Identifying differentially expressed genes using false discovery rate controlling procedures. *Bioinformatics*, 19(3):368–375.

Ritchie, M. E., Phipson, B., Wu, D., Hu, Y., Law, C. W., Shi, W., and Smyth, G. K. (2015). limma powers differential expression analyses for rna-sequencing and microarray studies. *Nucleic acids research*, 43(7):e47–e47.

Robert, C., Karaszewska, B., Schachter, J., Rutkowski, P., Mackiewicz, A., Stroiakovski, D., Lichinitser, M., Dummer, R., Grange, F., Mortier, L., et al. (2015). Improved overall survival in melanoma with combined dabrafenib and trametinib. *New England Journal of Medicine*, 372(1):30–39.

Rosenberg, T., Yeo, K. K., Mauguen, A., Alexandrescu, S., Prabhu, S. P., Tsai, J. W., Malinowski, S., Joshirao, M., Parikh, K., Farouk Sait, S., et al. (2022). Upfront molecular targeted therapy for the treatment of braf-mutant pediatric high-grade glioma. *Neuro-oncology*, 24(11):1964–1975.

Ryu, S., Woody, N., Chang, G., Mathialagan, S., and Varma, M. V. (2022). Identification of organic anion transporter 2 inhibitors: screening, structure-based analysis, and clinical drug interaction risk assessment. *Journal of Medicinal Chemistry*, 65(21):14578–14588.

Sasame, J., Ikegaya, N., Kawazu, M., Natsumeda, M., Hayashi, T., Isoda, M., Satomi, K., Tomiyama, A., Oshima, A., Honma, H., et al. (2022). Hsp90 inhibition overcomes resistance to molecular targeted therapy in brafv600e-mutant high-grade glioma. *Clinical Cancer Research*, 28(11):2425–2439.

Satyanarayana, A., Gudmundsson, K. O., Chen, X., Coppola, V., Tessarollo, L., Keller, J. R., and Hou, S. X. (2010). Rapgef2 is essential for embryonic hematopoiesis but dispensable for adult hematopoiesis. *Blood, The Journal of the American Society of Hematology*, 116(16):2921–2931.

Schreck, K. C., Langat, P., Bhave, V. M., Li, T., Woodward, E., Pratilas, C. A., Eberhart, C. G., and Bi, W. L. (2023). Integrated molecular and clinical analysis of braf-mutant glioma in adults. *NPJ Precision Oncology*, 7(1):23.

Schreck, K. C., Morin, A., Zhao, G., Allen, A. N., Flannery, P., Glantz, M., Green, A. L., Jones, C., Jones, K. L., Kilburn, L. B., Nazemi, K. J., Samuel, D., Sanford, B., Solomon, D. A., Wang, J., Pratilas, C. A., Nicolaides, T., and Mulcahy Levy, J. M. (2021). Deconvoluting Mechanisms of Acquired Resistance to RAF Inhibitors in BRAFV600E-Mutant Human Glioma. *Clinical Cancer Research*, 27(22):6197–6208.

Seaby, E. G., Pengelly, R. J., and Ennis, S. (2016). Exome sequencing explained: a practical guide to its clinical application. *Briefings in functional genomics*, 15(5):374–384.

Shi, G. and Zhang, Z. (2021). Rap2b promotes the proliferation and migration of human glioma cells via activation of the erk pathway. *Oncology Letters*, 21(4):1–10.

Smalley, I. and Smalley, K. S. (2018). Erk inhibition: a new front in the war against mapk pathway–driven cancers? *Cancer Discovery*, 8(2):140–142.

Smyth, G. K. (2005). Limma: linear models for microarray data. In *Bioinformatics and computational biology solutions using R and Bioconductor*, pages 397–420. Springer.

Sosman, J. A., Kim, K. B., Schuchter, L., Gonzalez, R., Pavlick, A. C., Weber, J. S., McArthur, G. A., Hutson, T. E., Moschos, S. J., Flaherty, K. T., et al. (2012). Survival in braf v600–mutant advanced melanoma treated with vemurafenib. *New England Journal of Medicine*, 366(8):707–714.

Subramanian, A., Tamayo, P., Mootha, V. K., Mukherjee, S., Ebert, B. L., Gillette, M. A., Paulovich, A., Pomeroy, S. L., Golub, T. R., Lander, E. S., et al. (2005). Gene set enrichment analysis: a knowledge-based approach for interpreting genome-wide

expression profiles. *Proceedings of the National Academy of Sciences*, 102(43):15545–15550.

Tabernero, J., Garcia-Carbonero, R., Cassidy, J., Sobrero, A., Van Cutsem, E., Köhne, C.-H., Tejpar, S., Gladkov, O., Davidenko, I., Salazar, R., et al. (2013). Sorafenib in combination with oxaliplatin, leucovorin, and fluorouracil (modified folfox6) as first-line treatment of metastatic colorectal cancer: the respect trial. *Clinical Cancer Research*, 19(9):2541–2550.

Taub, N., Teis, D., Ebner, H., Hess, M., and Huber, L. (2007). Late endosomal traffic of the epidermal growth factor receptor ensures spatial and temporal fidelity of mitogen-activated protein kinase signaling. *Molecular biology of the cell*, 18(12):4698–4710.

the Gene Ontology (2025). response to toxic substance. https://amigo.geneontology.org/amigo/term/GO:0009636 [Accessed: February 2025].

Tian, J., Liu, Y., Zhu, B., Tian, Y., Zhong, R., Chen, W., Lu, X., Zou, L., Shen, N., Qian, J., et al. (2015). Sf3a1 and pancreatic cancer: new evidence for the association of the spliceosome and cancer. *Oncotarget*, 6(35):37750.

Tomlinson, R. L., Ziegler, T. D., Supakorndej, T., Terns, R. M., and Terns, M. P. (2006). Cell cycle-regulated trafficking of human telomerase to telomeres. *Molecular biology of the cell*, 17(2):955–965.

Tong, R., Feng, L., Zhang, L., Zhang, J., Mao, Y., Zhang, K., Gao, Y., Wang, G., and Cheng, S. (2015). Decreased interferon alpha/beta signature associated with human lung tumorigenesis. *Journal of Interferon & Cytokine Research*, 35(12):963–968.

Twist Bioscience (2018a). Exome sequencing 101: Part 1 - library preparation. https://www.twistbioscience.com/blog/science/exome-sequencing-101-part-1-library-preparation [Accessed: November 2024].

Twist Bioscience (2018b). Exome sequencing 101: Part 2 - target enrichment. https://www.twistbioscience.com/blog/science/exome-sequencing-101-part-2-target-enrichment [Accessed: November 2024].

Twist Bioscience (2018c). Exome sequencing 101: Part 3 - next-generation sequencing (ngs). https://www.twistbioscience.com/blog/science/exome-sequencing-101-part-3-next-generation-sequencing-ngs [Accessed: November 2024].

Ura, H., Togi, S., and Niida, Y. (2022). A comparison of mrna sequencing (rna-seq) library preparation methods for transcriptome analysis. *BMC genomics*, 23(1):303.

Vakana, E., Pratt, S., Blosser, W., Dowless, M., Simpson, N., Yuan, X., Jaken, S., Manro, J., Stephens, J., Zhang, Y., et al. (2017). Ly3009120, a panraf inhibitor, has significant anti-tumor activity in braf and kras mutant preclinical models of colorectal cancer. oncotarget. 2017; 8: 9251–66. *DOI: https://doi. org/10.18632/oncotarget*, 14002:9251–9266.

Wang, J., Yao, Z., Jonsson, P., Allen, A. N., Qin, A. C. R., Uddin, S., Dunkel, I. J., Petriccione, M., Manova, K., Haque, S., et al. (2018). A secondary mutation in braf confers resistance to raf inhibition in a braf v600e-mutant brain tumor. *Cancer discovery*, 8(9):1130–1141.

Wang, P., Zhu, Y., Jia, X., Ying, X., Sun, L., and Ruan, S. (2023). Clinical prognostic value of osgin2 in gastric cancer and its proliferative effect in vitro. *Scientific Reports*, 13(1):5775.

West, S. and Proudfoot, N. J. (2009). Transcriptional termination enhances protein expression in human cells. *Molecular cell*, 33(3):354–364.

Wu, P.-K. and Park, J.-I. (2015). Mek1/2 inhibitors: molecular activity and resistance mechanisms. In *Seminars in oncology*, volume 42, pages 849–862. Elsevier.

Yamaguchi, H. and Condeelis, J. (2007). Regulation of the actin cytoskeleton in cancer cell migration and invasion. *Biochimica et Biophysica Acta (BBA)-Molecular Cell Research*, 1773(5):642–652.

Yang, Z., Wu, S., Fontana, F., Li, Y., Xiao, W., Gao, Z., Krudewig, A., Affolter, M., Belting, H.-G., Abdelilah-Seyfried, S., et al. (2021). The tight junction protein claudin-5 limits endothelial cell motility. *Journal of cell science*, 134(1):jcs248237.

Yao, Z., Torres, N. M., Tao, A., Gao, Y., Luo, L., Li, Q., de Stanchina, E., Abdel-Wahab, O., Solit, D. B., Poulikakos, P. I., et al. (2015). Braf mutants evade erk-dependent feedback by different mechanisms that determine their sensitivity to pharmacologic inhibition. *Cancer cell*, 28(3):370–383.

Yao, Z., Yaeger, R., Rodrik-Outmezguine, V. S., Tao, A., Torres, N. M., Chang, M. T., Drosten, M., Zhao, H., Cecchi, F., Hembrough, T., et al. (2017). Tumours with class 3 braf mutants are sensitive to the inhibition of activated ras. *Nature*, 548(7666):234–238.

Zhao, D., Yuan, H., Fang, Y., Gao, J., Li, H., Li, M., Cong, H., Zhang, C., Liang, Y., Li, J., et al. (2023). Histone methyltransferase kmt2b promotes metastasis and angiogenesis of cervical cancer by upregulating egf expression. *International Journal of Biological Sciences*, 19(1):34.

A. Appendix

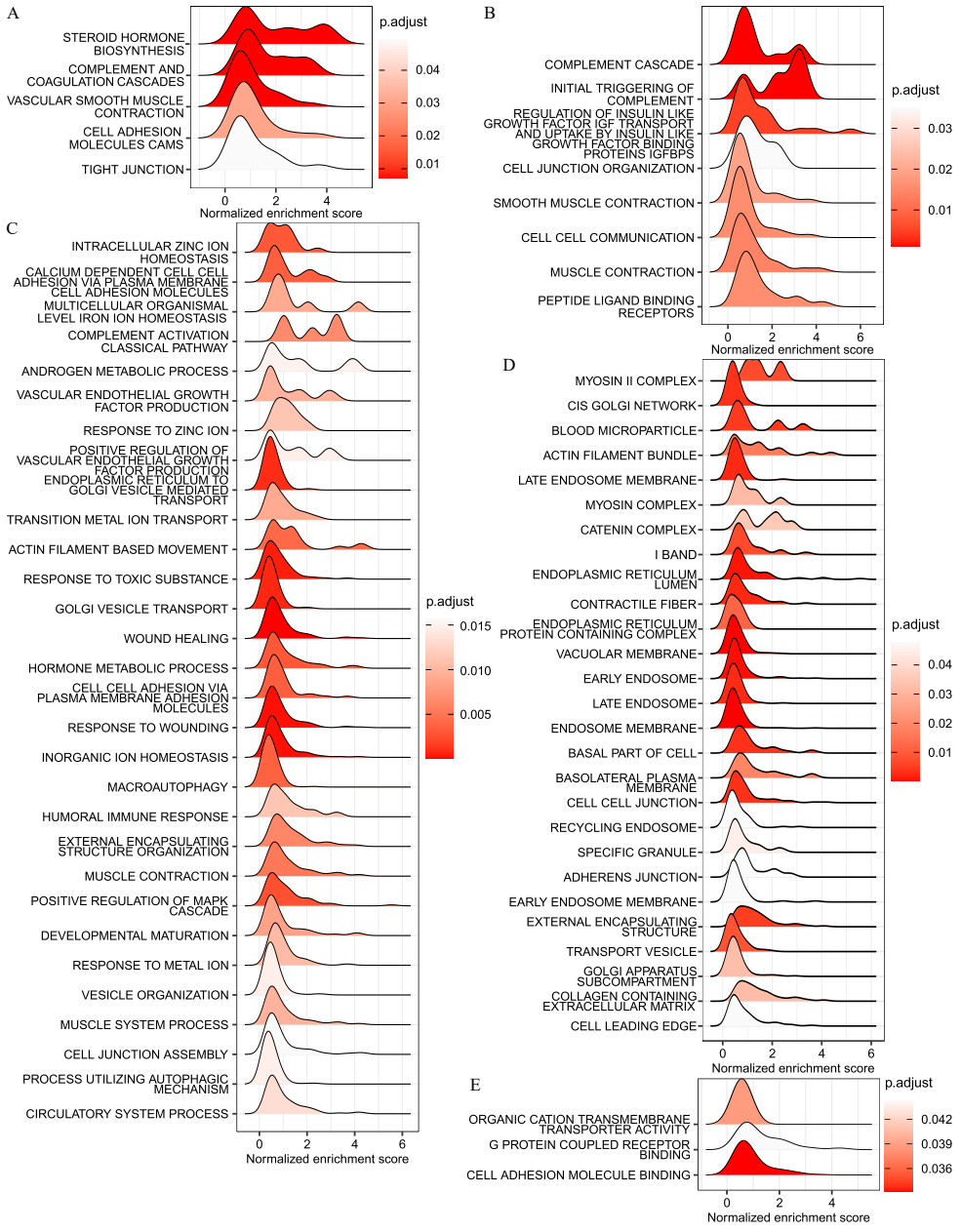

Figure A.1.: Ridgeline plots of unsupervised GSEA results of expression array data with VBT125Dabra versus VBT125 filtered by p.adjust < 0.05 and NES above zero. (A) KEGG_LEGACY, (B) REACTOME, (C) GOBP, (D) GOCC, (E) GOMF

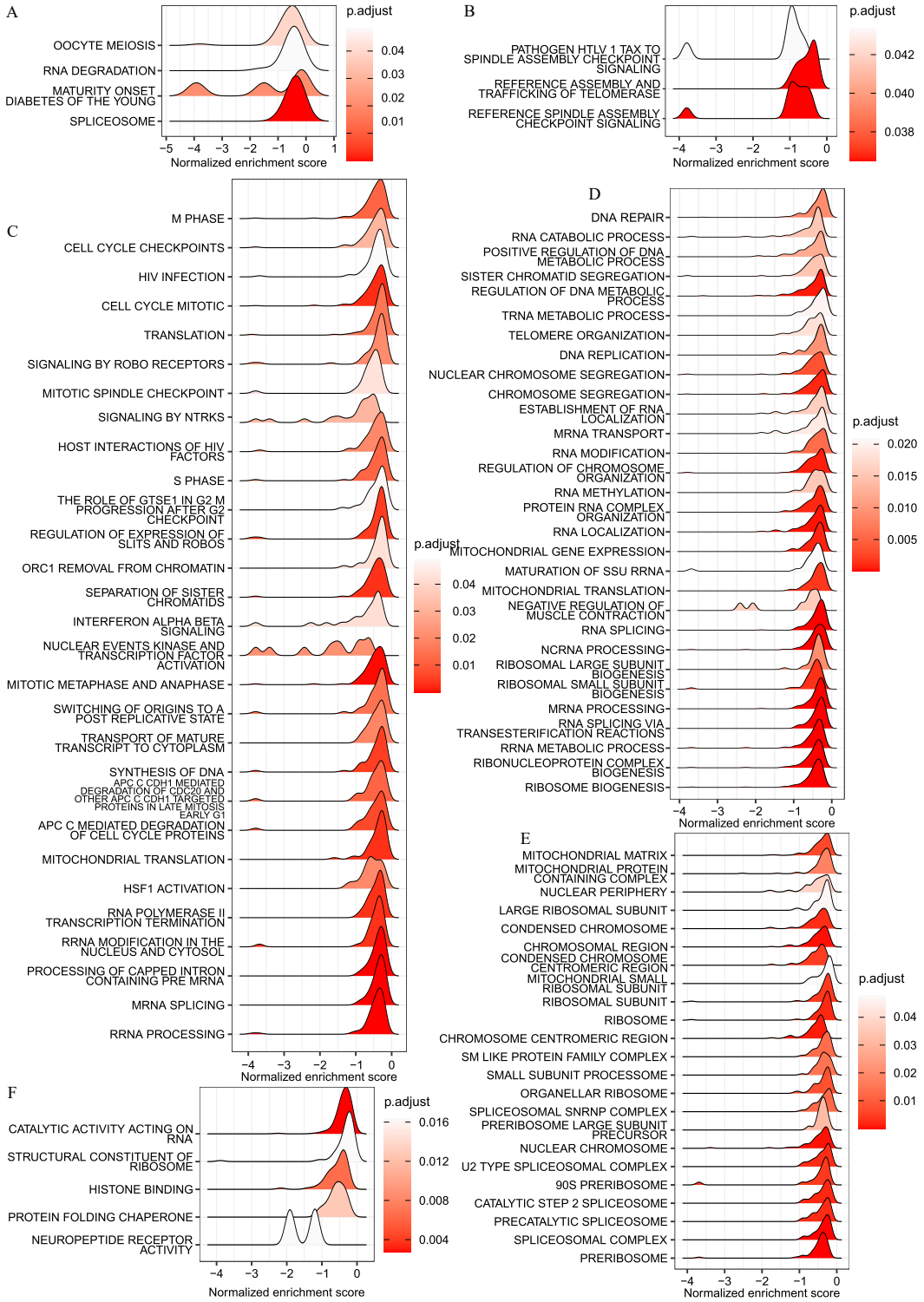

Figure A.2.: Ridgeline plots of unsupervised GSEA results of expression array data with VBT125Dabra versus VBT125 filtered by p.adjust < 0.05 and NES below zero. (A) KEGG_LEGACY, (B) KEGG_MEDICUS (C) REACTOME, (D) GOBP, (E) GOCC, (F) GOMF

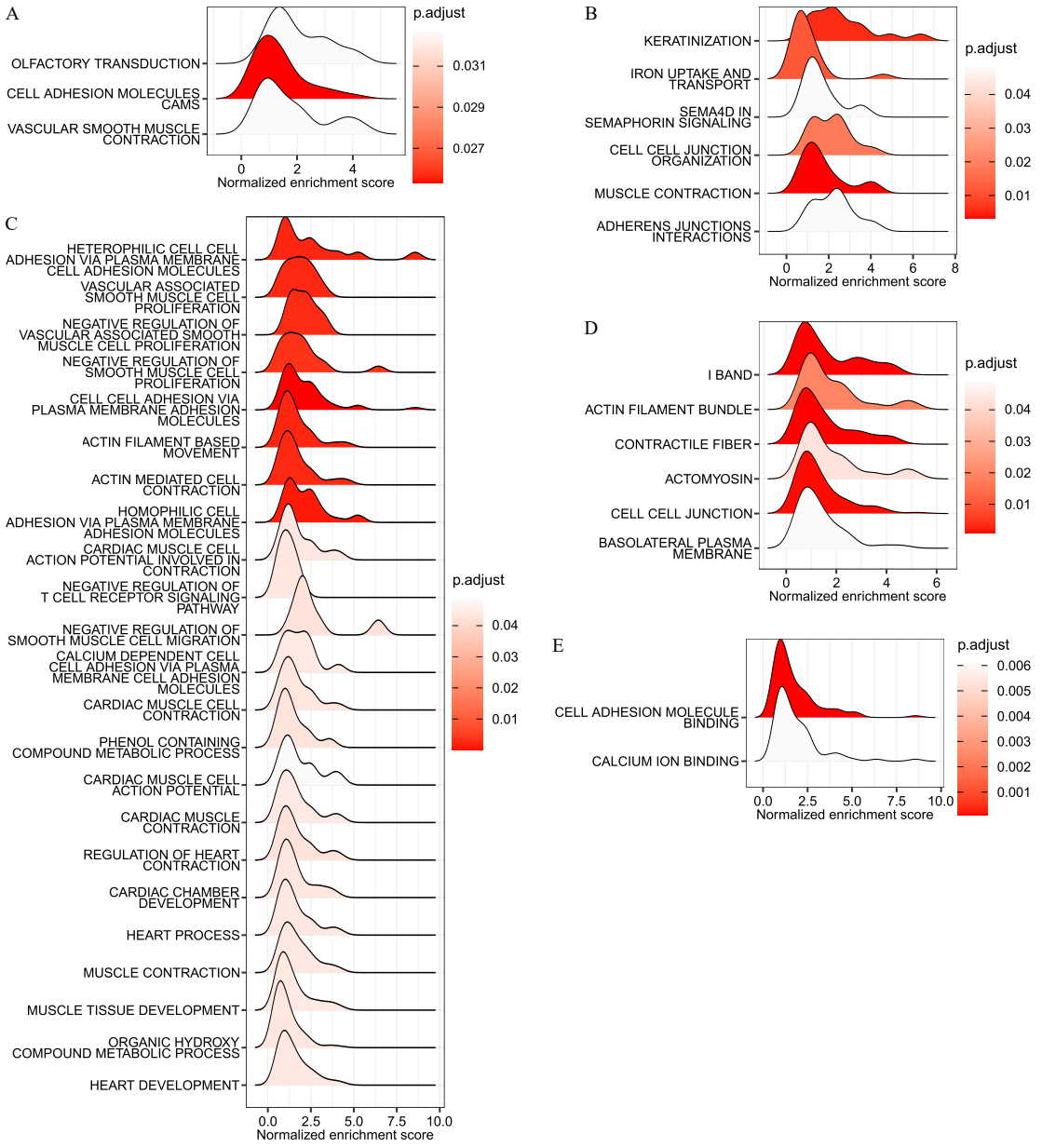

Figure A.3.: Ridgeline plots of unsupervised GSEA results of RNA seq data with VBT125Dabra versus VBT125 filtered by p.adjust < 0.05 and NES above zero. (A) KEGG_LEGACY, (B) REACTOME, (C) GOBP, (D) GOCC, (E) GOMF

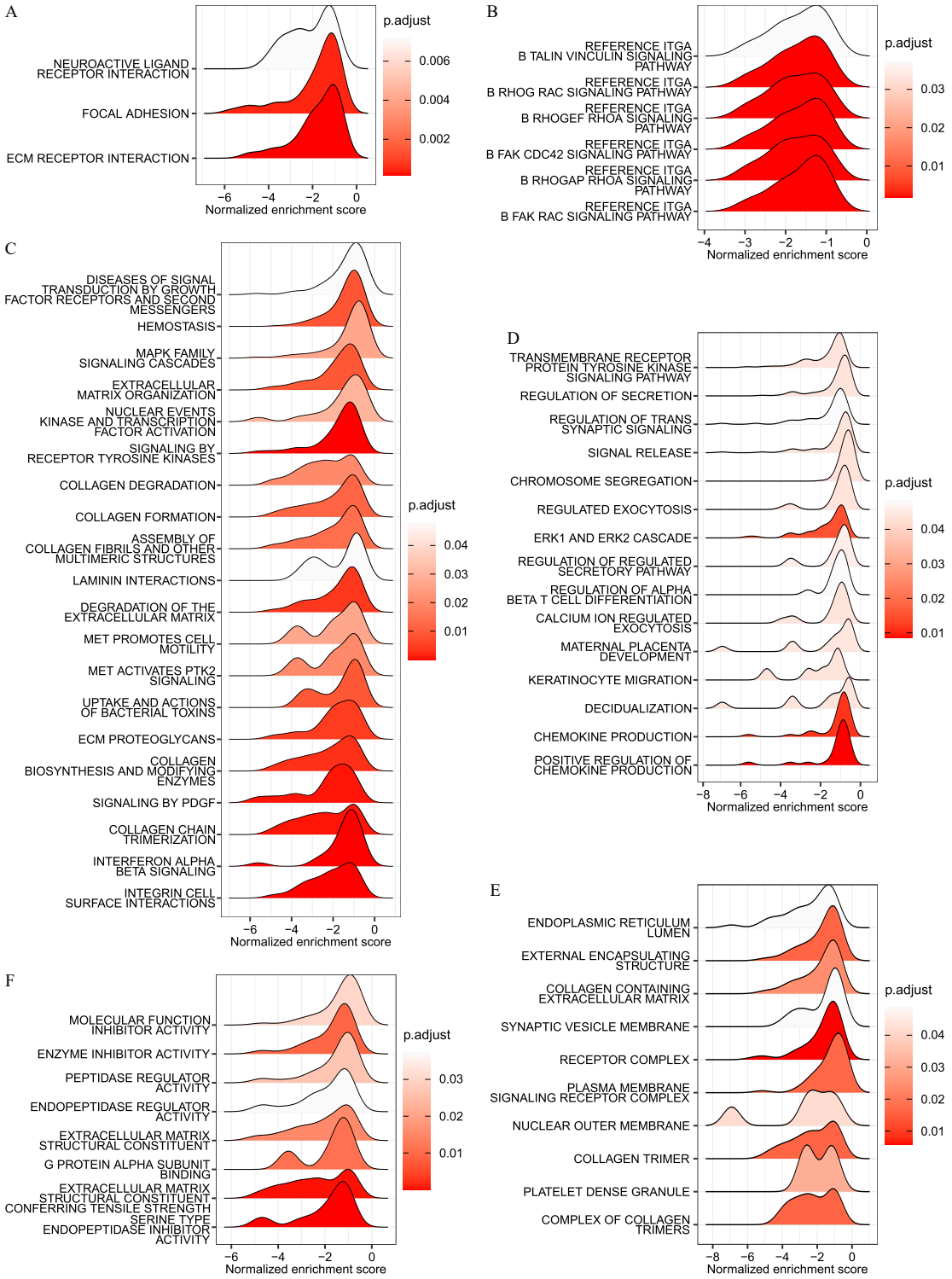

Figure A.4.: Ridgeline plots of unsupervised GSEA results of RNA seq data with VBT125Dabra versus VBT125 filtered by p.adjust < 0.05 and NES below zero. (A) KEGG_LEGACY, (B) KEGG_MEDICUS (C) REACTOME, (D) GOBP, (E) GOCC, (F) GOMF